Generalized Fourier Diffraction Theorem and Filtered Backpropagation for Tomographic Reconstruction

Clemens Kirisits[1,4]
clemens.kirisits@univie.ac.at

Michael Quellmalz[2]
quellmalz@math.tu-berlin.de

Eric Setterqvist[3]
eric.setterqvist@santa-anna.se

October 31, 2024

[1]Faculty of Mathematics
University of Vienna
Oskar-Morgenstern-Platz 1
A-1090 Vienna, Austria

[2]Institute of Mathematics
Technical University Berlin
Straße des 17. Juni 136
D-10623 Berlin, Germany

[3]Santa Anna IT Research Institute
SE-58183 Linköping, Sweden

[4]Christian Doppler Laboratory for
Mathematical Modeling and Simulation of
Next-Generation Ultrasound Devices (MaMSi)
Oskar-Morgenstern-Platz 1
A-1090 Vienna, Austria

Abstract

This paper concerns diffraction-tomographic reconstruction of an object characterized by its scattering potential. We establish a rigorous generalization of the Fourier diffraction theorem in arbitrary dimension, giving a precise relation in the Fourier domain between measurements of the scattered wave and reconstructions of the scattering potential. With this theorem at hand, Fourier coverages for different experimental setups are investigated taking into account parameters such as object orientation, direction of incidence and frequency of illumination. Allowing for simultaneous and discontinuous variation of these parameters, a general filtered backpropagation formula is derived resulting in an explicit approximation of the scattering potential for a large class of experimental setups.

1. Introduction

The Helmholtz equation. We consider an inverse source problem for the Helmholtz equation

$$-(\Delta + k_0^2)u = g \quad \text{in } \mathbb{R}^d, \tag{1.1}$$

where k_0 is a positive constant and g an integrable function with compact support. Given measurements of the unique outgoing solution u, the aim is to reconstruct g. Our first result connects the Fourier transform of g with that of u restricted to a hyperplane and may be seen as a generalization of the well-known Fourier diffraction theorem [21, 38, 48]. Let $\tilde{\mathcal{F}}\colon \mathcal{S}'(\mathbb{R}^d) \to \mathcal{S}'(\mathbb{R}^d)$

be the partial Fourier transform along the first $(d-1)$ coordinates. Then, $\tilde{\mathcal{F}}u$ is a locally integrable function given by

$$\tilde{\mathcal{F}}u(\mathbf{x}, r_{\mathrm{M}}) = \sqrt{\frac{\pi}{2}}\frac{\mathrm{i}}{\kappa}\left(\mathrm{e}^{\mathrm{i}\kappa r_{\mathrm{M}}}\mathcal{F}(g^-)(\mathbf{x},\kappa) + \mathrm{e}^{-\mathrm{i}\kappa r_{\mathrm{M}}}\mathcal{F}(g^+)(\mathbf{x},-\kappa)\right), \quad \mathbf{x}\in\mathbb{R}^{d-1},\ r_{\mathrm{M}}\in\mathbb{R}, \tag{1.2}$$

where $\kappa = \kappa(\mathbf{x})$ is the principal square root of $k_0^2 - |\mathbf{x}|^2$ and $\mathcal{F}$ is the Fourier transform on $\mathbb{R}^d$, continued analytically to $\mathbb{C}^d$ for $|\mathbf{x}|^2 > k_0^2$. The functions g^+ and g^- are defined by $g^{\pm}(\mathbf{r}) = g(\mathbf{r})$ if $r_d \gtrless r_{\mathrm{M}}$ and $g^{\pm}(\mathbf{r}) = 0$ otherwise. Assuming that u is measured on the hyperplane $\{\mathbf{r}\in\mathbb{R}^d : r_d = r_{\mathrm{M}}\}$, then (1.2) relates the spatial frequency components of the data to those of g^+ and g^-.

Theorem 3.3 where (1.2) is proved generalizes [28, Thm. 3.1], which covers only the case $d = 3$ and requires the compactly supported inhomogeneity g to belong to $L^p(\mathbb{R}^3)$ with $p > 1$. The stricter condition on g in [28, Thm. 3.1] is a consequence of the dependency on integrability estimates of u, see Remark 2.3, in its proof. In contrast, the proof of Theorem 3.3 relies on a certain continuity of the map $g \mapsto u$ established in Theorem 2.4 for which the weaker assumption $g \in L^1(\mathbb{R}^d)$ is sufficient. There exist many other formulations of the Fourier diffraction theorem in $d \in \{2, 3\}$ such as [5, 9, 21, 37, 38, 48] that only consider the plane wave case discussed in the following paragraph. Among these references, [38] imposes the stronger assumption that $g \in L^2(\mathbb{R}^d)$, while the others do not state the conditions explicitly. In general, the derivations in the above cited references are based on the plane wave decomposition of the Green's function of the Helmholtz equation. The proof of Theorem 3.3 on the other hand is done in the framework of tempered distributions with the major component being, besides Theorem 2.4, the partial Fourier transform of the Green's function given in Lemma 3.2.

Diffraction tomography. The Helmholtz equation (1.1) arises as a model for the scattering of time-harmonic waves $U(\mathbf{r}, t) = \mathrm{Re}(u^{\mathrm{tot}}(\mathbf{r})\mathrm{e}^{-\mathrm{i}\omega t})$ from a bounded inhomogeneity. Assuming that the wave motion is caused by an incident field u^{inc} propagating through a homogeneous background until it meets the scatterer, a common model for the resulting scattered field $u^{\mathrm{sca}} = u^{\mathrm{tot}} - u^{\mathrm{inc}}$ is

$$-(\Delta + k_0^2)u^{\mathrm{sca}} = k_0^2 f u^{\mathrm{tot}} \quad \text{in } \mathbb{R}^d. \tag{1.3}$$

In addition, u^{sca} satisfies the Sommerfeld radiation condition, see [7, Chap. 8.1]. In this context, $k_0 > 0$ is the wave number of the incident field u^{inc}, which is assumed to solve $\Delta u^{\mathrm{inc}} + k_0^2 u^{\mathrm{inc}} = 0$, and the normalized scattering potential f is given by

$$f(\mathbf{r}) = \frac{n(\mathbf{r})^2}{n_0^2} - 1, \quad \mathbf{r}\in\mathbb{R}^d, \tag{1.4}$$

where n is the refractive index. Outside the bounded inhomogeneity, we have $n(\mathbf{r}) \equiv n_0$, so f is compactly supported. In general f has a nonzero imaginary part in order to allow for absorption.

Two common simplifications of this scattering model are the Born and the Rytov approximation, each leading to an equation of the form (1.1). The first-order Born approximation neglects the term $k_0^2 f u^{\mathrm{sca}}$ on the right-hand side of (1.3) and reads

$$-(\Delta + k_0^2)u^{\mathrm{sca}} = k_0^2 f u^{\mathrm{inc}}. \tag{1.5}$$

The first-order Rytov approximation is based on the ansatz $u^{\mathrm{tot}} = u^{\mathrm{inc}}\mathrm{e}^{\varphi}$ with a complex phase function φ and leads to

$$-(\Delta + k_0^2)(u^{\mathrm{inc}}\varphi) = k_0^2 f u^{\mathrm{inc}}. \tag{1.6}$$

Further details on the derivation and validity of these approximations can be found, for instance, in [21, Chap. 6] and also [13]. Within this framework, the inverse problem of diffraction tomography,

see [10, 21, 38], can be formulated as follows: Given knowledge of the incident field u^{inc} as well as measurements of the scattered wave on a hyperplane in $\mathbb{R}^d$, recover the scattering potential f based on (1.5) or (1.6).

A key result underlying diffraction tomography, the Fourier diffraction theorem, can be obtained as a special case of (1.2) by setting $g = k_0^2 f u^{\text{inc}}$, see (1.5), and assuming that (i) measurements are taken outside the support of f and (ii) the incident field is a plane wave $u^{\text{inc}}(\mathbf{r}) = \mathrm{e}^{ik_0\mathbf{r}\cdot\mathbf{s}}$ propagating in direction $\mathbf{s} \in \mathbb{S}^{d-1}$. Then (1.2) becomes the more familiar

$$\tilde{\mathcal{F}}u(\mathbf{x}, r_{\text{M}}) = \sqrt{\frac{\pi}{2}}\,\frac{\mathrm{i}k_0^2 \mathrm{e}^{\pm \mathrm{i}\kappa r_{\text{M}}}}{\kappa}\mathcal{F}f\left((\mathbf{x}, \pm\kappa) - k_0\mathbf{s}\right) \quad \text{if } r_{\text{M}} \gtrless r_d \text{ for all } \mathbf{r} \in \operatorname{supp} f. \tag{1.7}$$

Note that (1.2) can be used to obtain a relation between scattered wave and scattering potential even when u^{inc} is not a plane wave, see Remark 4.2.

In applications, mainly the spatial frequencies $\mathbf{x} \in \mathbb{R}^{d-1}$ with $|\mathbf{x}| < k_0$ are relevant. This provides information about $\mathcal{F}f$ at the points $(\mathbf{x}, \pm\kappa(\mathbf{x})) - k_0\mathbf{s}$ on a sphere in $\mathbb{R}^d$ with radius k_0 and center $-k_0\mathbf{s}$. Knowledge of $\mathcal{F}f$ on this set only is not sufficient for a reasonable recovery of f. Therefore, reconstruction algorithms in diffraction tomography crucially rely on data collection strategies gathering additional information by varying one or more of the following parameters of the experiment: (i) the direction $\mathbf{s}$ of the incident wave, (ii) the orientation of the scatterer described by a rotation matrix $R \in SO(d)$, or (iii) the wave number k_0 of u^{inc}. In Section 4, we investigate how changes in each of these parameters (plus additional ones which are shown to be ineffective) influence the coverage in Fourier space. A general experiment, where all parameters are allowed to change simultaneously depending on time $t \in [0, L]$, leads in $\mathbb{R}^d$ to the Fourier coverage

$$\mathcal{Y} = \left\{ R(t)\left((\mathbf{x}, \pm\kappa(\mathbf{x}, t)) - k_0(t)\,\mathbf{s}(t)\right) \in \mathbb{R}^d : 0 \leqslant t \leqslant L,\ |\mathbf{x}| < k_0(t) \right\},$$

where κ depends on t through k_0.

Filtered backpropagation. Filtered backpropagation, as pioneered in [9], provides an explicit reconstruction formula for

$$f_{\mathcal{Y}}(\mathbf{r}) := (2\pi)^{-\frac{d}{2}} \int_{\mathcal{Y}} \mathcal{F}f(\mathbf{y}) \mathrm{e}^{\mathrm{i}\mathbf{r}\cdot\mathbf{y}}\,\mathrm{d}\mathbf{y}$$

for every $\mathbf{r} \in \mathbb{R}^d$. The idea is to first apply the change of coordinates

$$\mathbf{y} = T(\mathbf{x}, t) := R(t)\left((\mathbf{x}, \kappa(\mathbf{x}, t)) - k_0(t)\,\mathbf{s}(t)\right),$$

and then use the Fourier diffraction theorem (1.7) to replace the spatial frequency components of f with those of the measurements u. One issue with this approach is that T is far from injective in general. Therefore, in order to correctly extend filtered backpropagation formulas to the general setting proposed here, one has to account for the lack of injectivity by means of the Banach indicatrix

$$\operatorname{Card}\left(T^{-1}(\mathbf{y})\right),$$

where Card denotes the counting measure. While the Banach indicatrix can be difficult to determine in general, we suggest a numerical procedure for estimating it.

Another issue, not only with filtered backpropagation but with diffraction tomographic methods in general, is the missing cone problem, cf. [29, 32, 33, 47]. This is the observation that for many experimental setups the Fourier coverage has significant cone-like holes close to the origin, see Figure 2 or Figure 5, for example. Consequently, a considerable portion of the low spatial

frequencies of f is not available for reconstruction, thus leading to poor results. The missing cone problem can be overcome, for instance, by consecutively rotating the object around more than one axis or by subsequently illuminating from more than one direction during rotation. In order to correctly incorporate the resulting measurements into a single backpropagation formula, we allow the functions $R(t)$, $\mathbf{s}(t)$ and $k_0(t)$, and hence T, to have jump discontinuities. We establish the corresponding backpropagation formula allowing for noninjective and discontinuous T in Theorem 5.4. Subsequently, we present an improvement of this formula for real-valued f that exploits the conjugate symmetry of $\hat{f}$ and ensures that the reconstruction $f_{\mathcal{Y}}$ is real-valued as well. In general, it enlarges the Fourier coverage while reducing the amount of data required to achieve a certain coverage. Numerical tests show that the new backpropagation method can provide a reconstruction quality similar to the inverse NDFT method while being faster. The speed advantage becomes especially relevant when the reconstruction is used inside an iterative method such as for phase retrieval, see [2, 3], where the Banach indicatrix needs to be computed only once.

Outline. This article is organized as follows. After reviewing certain results concerning the well-posedness of the forward problem $g \mapsto u$ associated to (1.1) in Section 2, we prove the generalized Fourier diffraction theorem in Section 3. Section 4 is devoted to the systematic study of Fourier coverages resulting from various experimental setups. A universal filtered backpropagation formula together with some extensions and special cases is derived in Section 5. Finally, the discretization is discussed in Section 6.1, where we also present an estimation method of the Banach indicatrix. Numerical experiments are performed in Section 6.2.

2. The Helmholtz equation in $\mathbb{R}^d$

In this section we recall results concerning outgoing solutions to the Helmholtz equation

$$-(\Delta + k_0^2)u(\mathbf{r}) = g(\mathbf{r}), \quad \mathbf{r} \in \mathbb{R}^d, \tag{2.1}$$

for compactly supported g. A solution u of (2.1) is *outgoing,* if it satisfies the *Sommerfeld radiation condition*

$$\lim_{r\to\infty} r^{\frac{d-1}{2}} \left(\frac{\partial u}{\partial r} - \mathrm{i}k_0 u \right) = 0 \tag{2.2}$$

uniformly in $\mathbf{s}$, where $\mathbf{r} = r\mathbf{s}$, $r = |\mathbf{r}|$, and $\partial/\partial r$ denotes the radial derivative. The significance of the Sommerfeld radiation condition is twofold. First, it characterizes outgoing waves. That is, if u satisfies (2.1) and (2.2), then $U(\mathbf{r}, t) = \operatorname{Re}\left(u(\mathbf{r})\mathrm{e}^{-\mathrm{i}\omega t}\right)$, $\omega > 0$, physically corresponds to a wave propagating away from the scatterer [8, Chap. IV, §5]. Second, the Sommerfeld radiation condition ensures uniqueness for (2.1), see Theorem 2.1. Due to the hypoellipticity of $\Delta + k_0^2$, every distributional solution u of (2.1) is smooth on $\mathbb{R}^d \setminus \operatorname{supp} g$, so that the differentiability requirement implicit in (2.2) is always met for compactly supported g, see [15].

We denote the space of test functions by $\mathcal{D}(\mathbb{R}^d)$, which consists of all compactly supported smooth functions, and the space of distributions by $\mathcal{D}'(\mathbb{R}^d)$. Furthermore, we will need the Schwartz space $\mathcal{S}(\mathbb{R}^d)$ of rapidly decreasing, smooth functions and the space of tempered distributions $\mathcal{S}'(\mathbb{R}^d)$.

An outgoing fundamental solution of the d-dimensional Helmholtz operator $-\Delta - k_0^2$ is given by

$$G(\mathbf{r}) = \frac{\mathrm{i}}{4} \left(\frac{k_0}{2\pi|\mathbf{r}|} \right)^{\frac{d-2}{2}} H^{(1)}_{\frac{d-2}{2}}(k_0 |\mathbf{r}|), \tag{2.3}$$

where $H_a^{(1)}$ is the Hankel function of the first kind and order a. See [35, Chap. 9] for a derivation of (2.3). The function G is also known as Green's function for the Helmholtz equation. Note that $G \in C^\infty(\mathbb{R}^d \backslash \{0\})$. Moreover, the limiting forms

$$H_a^{(1)}(z) \sim \begin{cases} -\frac{\mathrm{i}}{\pi}\Gamma(a)\left(\frac{z}{2}\right)^{-a}, & \operatorname{Re} a > 0, \\ \frac{2\mathrm{i}}{\pi}\log(z), & a = 0, \end{cases} \qquad \text{for} \quad z \to 0, \tag{2.4}$$

and

$$H_a^{(1)}(z) \sim \sqrt{\frac{2}{\pi z}}\mathrm{e}^{\mathrm{i}\left(z - \frac{a\pi}{2} - \frac{\pi}{4}\right)}, \qquad \text{for} \quad z \to \infty, \tag{2.5}$$

imply that G belongs to $L^1_{\mathrm{loc}}(\mathbb{R}^d) \cap \mathcal{S}'(\mathbb{R}^d)$ and that

$$G(\mathbf{r}) = \mathcal{O}\left(|\mathbf{r}|^{\frac{1-d}{2}}\right), \qquad \text{for} \quad |\mathbf{r}| \to \infty, \tag{2.6}$$

see [39, (10.2.5), (10.7.2), (10.7.7)]. Concerning tomographic reconstructions in the two- and three-dimensional space, notable special cases of (2.3) are

$$G(\mathbf{r}) = \begin{cases} \dfrac{\mathrm{i}\mathrm{e}^{\mathrm{i}k_0|\mathbf{r}|}}{2k_0}, & d = 1, \\ \dfrac{\mathrm{i}}{4}H_0^{(1)}(k_0\,|\mathbf{r}|), & d = 2, \\ \dfrac{\mathrm{e}^{\mathrm{i}k_0|\mathbf{r}|}}{4\pi|\mathbf{r}|}, & d = 3. \end{cases} \tag{2.7}$$

The following theorem shows that outgoing solutions of (2.1) are unique in $\mathcal{D}'(\mathbb{R}^d)$ and that, in particular, G is unique. Related results are [43, 46]. See also [8, Chap. IV, §5] or [35, Thm. 9.11].

Theorem 2.1 *For every $g \in \mathcal{D}'(\mathbb{R}^d)$ with compact support, there is at most one outgoing solution of (2.1).*

Proof: Suppose $u \in \mathcal{D}'(\mathbb{R}^d)$ is an outgoing solution of (2.1). Every other solution of (2.1) can be written as $u + v$ where $\Delta v + k_0^2 v = 0$ on $\mathbb{R}^d$. But $u + v$ can only be outgoing, if v is. It now follows that v must vanish identically from Green's formula, also known as Green's third identity,

$$v(\mathbf{r}) = \int_{\partial B} v\nabla G_{\mathbf{r}} \cdot \mathbf{n} - G_{\mathbf{r}}\nabla v \cdot \mathbf{n}\,\mathrm{d}s, \tag{2.8}$$

where $\mathbf{r} \in \mathbb{R}^d$ is arbitrary, B is a closed ball not containing $\mathbf{r}$, $G_{\mathbf{r}}$ is a shorthand for $G(\mathbf{r} - \cdot)$ and $\mathbf{n}$ is the outward pointing unit normal. See [7, Thm. 2.5] for $d = 3$ or [35, Thms. 7.12, 9.6] for a more general formulation. Applying Green's second identity to (2.8) and exploiting the fact that both v and $G_{\mathbf{r}}$ solve the homogeneous Helmholtz equation in B shows that $v(\mathbf{r}) = 0$. ▫

Theorem 2.2 *For every $g \in L^1(\mathbb{R}^d)$ with compact support, $u = g * G \in L^1_{\mathrm{loc}}(\mathbb{R}^d) \cap \mathcal{S}'(\mathbb{R}^d)$ is the unique distributional solution of the Helmholtz equation (2.1) that satisfies the Sommerfeld radiation condition (2.2).*

Proof: First, $u = g * G$ solves (2.1) in the distributional sense, because G is a fundamental solution of $-\Delta - k_0^2$. Next, we show that $u \in L^1_{\mathrm{loc}}(\mathbb{R}^d) \cap \mathcal{S}'(\mathbb{R}^d)$. Take a compact set $K \subset \mathbb{R}^d$

and a bounded set $B \supset \operatorname{supp} g$. Using the Fubini–Tonelli theorem, local integrability of G and the Minkowski difference $K - B$, we obtain

$$\begin{aligned}\int_K |u(\mathbf{r})| \,\mathrm{d}\mathbf{r} &\leqslant \int_K \int_{\mathbb{R}^d} |g(\mathbf{y})G(\mathbf{r}-\mathbf{y})| \,\mathrm{d}\mathbf{y}\,\mathrm{d}\mathbf{r} \\ &= \int_{\mathbb{R}^d} |g(\mathbf{y})| \int_K |G(\mathbf{r}-\mathbf{y})| \,\mathrm{d}\mathbf{r}\,\mathrm{d}\mathbf{y} \\ &= \int_{\mathbb{R}^d} |g(\mathbf{y})| \int_{K-\mathbf{y}} |G(\mathbf{u})| \,\mathrm{d}\mathbf{u}\,\mathrm{d}\mathbf{y} \\ &\leqslant \int_{K-B} |G(\mathbf{u})| \,\mathrm{d}\mathbf{u} \int_B |g(\mathbf{y})| \,\mathrm{d}\mathbf{y} \\ &\leqslant \|G\|_{L^1(K-B)} \|g\|_{L^1(\mathbb{R}^d)} . \end{aligned} \tag{2.9}$$

Therefore, u is locally integrable. By (2.6), there exists a radius $R > 0$ and a constant $C > 0$ such that

$$|u(\mathbf{r})| \leqslant \int_B |g(\mathbf{y})G(\mathbf{r}-\mathbf{y})| \,\mathrm{d}\mathbf{y} \leqslant C \|g\|_{L^1(\mathbb{R}^d)} \tag{2.10}$$

when $|\mathbf{r}| > R$. So, u can be identified with a tempered distribution.

Concerning the Sommerfeld radiation condition let $\mathbf{r} \notin \operatorname{supp} g$. Then we have

$$\left| \frac{\partial u}{\partial r}(\mathbf{r}) - \mathrm{i}k_0 u(\mathbf{r}) \right| \leqslant \|g\|_{L^1} \sup_{\mathbf{y} \in \operatorname{supp} g} \left| \frac{\partial G}{\partial r}(\mathbf{r}-\mathbf{y}) - \mathrm{i}k_0 G(\mathbf{r}-\mathbf{y}) \right| .$$

Since $\operatorname{supp} g$ is compact, the right-hand side has the same asymptotic behavior for $|\mathbf{r}| \to \infty$ as $\partial G/\partial r(\mathbf{r}) - \mathrm{i}k_0 G(\mathbf{r})$. Therefore, u satisfies (2.2).

The uniqueness of u follows from Theorem 2.1. ▫

Remark 2.3 While Theorem 2.2 only asserts that $u = g * G$ is a distributional solution of (2.1), under slightly stronger assumptions it can be shown that u is actually a strong solution. Specifically, let $d \geqslant 2$ and $g \in L^r(\mathbb{R}^d)$ with $r > \max(1, 2d/(3+d))$ and compact support. Furthermore, let $p, q \geqslant 1$ satisfy

$$p \leqslant r, \quad \frac{d+1}{2d} < \frac{1}{p}, \quad \frac{1}{q} < \frac{d-1}{2d}, \quad \frac{2}{d+1} \leqslant \frac{1}{p} - \frac{1}{q} \leqslant \frac{2}{d}, \quad \frac{1}{p} - \frac{1}{q} < 1.$$

Then one can apply the estimate

$$\|\phi * G\|_{L^q(\mathbb{R}^d)} \leqslant C \|\phi\|_{L^p(\mathbb{R}^d)} , \quad \text{for all } \phi \in \mathcal{S}(\mathbb{R}^d),$$

from [24] (see also [12, Thm. 2.1] and [18, Thm. 6]) to conclude that $u \in L^q(\mathbb{R}^d)$. Using elliptic regularity theory, one can argue that $u \in W^{2,p}_{\mathrm{loc}}(\mathbb{R}^d)$, see [11, Prop. A.1].

The proof of Theorem 3.3 requires the following continuity result for the map $g \mapsto u$. It takes into account the compact support of g but otherwise requires less regularity than Remark 2.3. We denote by $\mathcal{B}^d_R$ the open ball in $\mathbb{R}^d$ centered at 0 with radius R.

Theorem 2.4 *If $g_n \to 0$ in $L^1(\mathbb{R}^d)$ and $\bigcup_n \operatorname{supp} g_n$ is bounded, then $g_n * G \to 0$ in $\mathcal{S}'(\mathbb{R}^d)$.*

Proof: Let $B = \bigcup_n \operatorname{supp} g_n$. There exists a sufficiently large $R > 0$ such that for any $\phi \in \mathcal{S}(\mathbb{R}^d)$ we obtain

$$\begin{aligned}\left|\int_{\mathbb{R}^d} g_n * G(\mathbf{r})\phi(\mathbf{r})\,\mathrm{d}\mathbf{r}\right| &\leqslant \int_{\mathcal{B}_R^d} |g_n * G(\mathbf{r})\phi(\mathbf{r})|\,\mathrm{d}\mathbf{r} + \int_{\mathbb{R}^d\setminus\mathcal{B}_R^d} |g_n * G(\mathbf{r})\phi(\mathbf{r})|\,\mathrm{d}\mathbf{r}\\ &\leqslant \left(\|G\|_{L^1(\mathcal{B}_R^d - B)}\,\|\phi\|_{L^\infty(\mathbb{R}^d)} + C\|\phi\|_{L^1(\mathbb{R}^d)}\right)\|g_n\|_{L^1(\mathbb{R}^d)},\end{aligned}$$

where we have used (2.9) for the first and (2.10) for the second integral. For $n \to \infty$, we conclude that

$$\int_{\mathbb{R}^d} g_n * G(\mathbf{r})\phi(\mathbf{r})\,\mathrm{d}\mathbf{r} \to 0$$

and therefore $G * g_n \to 0$ in $\mathcal{S}'$. ▫

3. A generalized Fourier diffraction theorem

We denote by $\mathcal{F}_j$ the partial Fourier transform with respect to the j-th coordinate. That is, if ϕ belongs to the Schwartz space $\mathcal{S}(\mathbb{R}^d)$, we define

$$\mathcal{F}_j\phi(r_1,\dots,r_{j-1},k_j,r_{j+1},\dots r_d) = (2\pi)^{-\frac{1}{2}}\int_{\mathbb{R}} \phi(\mathbf{r})\mathrm{e}^{-\mathrm{i}k_j r_j}\,\mathrm{d}r_j.$$

Note that $\mathcal{F}_j$ can be extended to a continuous linear bijection with continuous inverse on the space of tempered distributions $\mathcal{S}'(\mathbb{R}^d)$. The usual d-dimensional Fourier transform is given by $\mathcal{F} = \mathcal{F}_1 \circ \cdots \circ \mathcal{F}_d$. We also use the shorthand $\hat{g}$ for $\mathcal{F}g$.

If $d \geqslant 2$ the Fourier transform with respect to the first $d-1$ coordinates is abbreviated by

$$\tilde{\mathcal{F}} := \mathcal{F}_1 \circ \cdots \circ \mathcal{F}_{d-1}. \tag{3.1}$$

Similarly, for $\mathbf{r} \in \mathbb{R}^d$ we define the truncated vector $\tilde{\mathbf{r}} = (r_1,\dots,r_{d-1}) \in \mathbb{R}^{d-1}$. We also let

$$\kappa : \mathbb{R}^{d-1} \to \mathbb{C},\ \kappa(\tilde{\mathbf{r}}) := \begin{cases}\sqrt{k_0^2 - |\tilde{\mathbf{r}}|^2}, & |\tilde{\mathbf{r}}| \leqslant k_0,\\ \mathrm{i}\sqrt{|\tilde{\mathbf{r}}|^2 - k_0^2}, & |\tilde{\mathbf{r}}| > k_0.\end{cases} \tag{3.2}$$

Lemma 3.1 *Let $d \geqslant 2$. Then $1/\kappa \in L^1_{\mathrm{loc}}(\mathbb{R}^d)$ and $\phi \mapsto \int_{\mathbb{R}^d} \phi(\mathbf{r})/\kappa(\tilde{\mathbf{r}})\,\mathrm{d}\mathbf{r}$ is a tempered distribution.*

Proof: Concerning the first claim we have $|\kappa(\tilde{\mathbf{r}})| \geqslant \sqrt{k_0\,|k_0 - |\tilde{\mathbf{r}}||}$ and therefore, for every $R > 0$,

$$\int_{\mathcal{B}_R^{d-1}} \frac{\mathrm{d}\tilde{\mathbf{r}}}{|\kappa(\tilde{\mathbf{r}})|} \leqslant \int_{\mathcal{B}_R^{d-1}} \frac{\mathrm{d}\tilde{\mathbf{r}}}{\sqrt{k_0\,|k_0 - |\tilde{\mathbf{r}}||}} \leqslant C\int_0^R \frac{r^{d-2}\,\mathrm{d}r}{\sqrt{|k_0 - r|}} < +\infty. \tag{3.3}$$

This shows that $1/\kappa \in L^1_{\mathrm{loc}}(\mathbb{R}^{d-1})$ and consequently $1/\kappa \in L^1_{\mathrm{loc}}(\mathbb{R}^d)$ as well.

For the second claim let $R > k_0$. Then $|\kappa| \geqslant \sqrt{k_0(R-k_0)}$ on $S := \{\mathbf{r} \in \mathbb{R}^d : |\tilde{\mathbf{r}}| \geqslant R\}$, and for an arbitrary $\phi \in \mathcal{S}(\mathbb{R}^d)$ it follows that

$$\begin{aligned}\left|\int_{\mathbb{R}^d} \frac{\phi(\mathbf{r})}{\kappa(\tilde{\mathbf{r}})}\,\mathrm{d}\mathbf{r}\right| &= \left|\int_{\mathbb{R}}\int_{\mathcal{B}_R^{d-1}} \frac{\phi(\mathbf{r})}{\kappa(\tilde{\mathbf{r}})}\,\mathrm{d}\tilde{\mathbf{r}}\,\mathrm{d}x_d + \int_S \frac{\phi(\mathbf{r})}{\kappa(\tilde{\mathbf{r}})}\,\mathrm{d}\mathbf{r}\right| \\ &\leqslant \|1/\kappa\|_{L^1(\mathcal{B}_R^{d-1})} \int_{\mathbb{R}} \sup_{|\tilde{\mathbf{r}}|\leqslant R} |\phi(\tilde{\mathbf{r}}, x_d)|\,\mathrm{d}x_d + (k_0(R-k_0))^{-\frac{1}{2}} \int_S |\phi(\mathbf{r})|\,\mathrm{d}\mathbf{r} \\ &\leqslant C\left(\int_{\mathbb{R}} \sup_{|\tilde{\mathbf{r}}|\leqslant R} |\phi(\mathbf{r})|\,\mathrm{d}x_d + \int_{\mathbb{R}^d} |\phi(\mathbf{r})|\,\mathrm{d}\mathbf{r}\right).\end{aligned}$$

Both of these integrals can be bounded by appropriate seminorms on $\mathcal{S}(\mathbb{R}^d)$. For the second one we recall that $\mathcal{S}(\mathbb{R}^d)$ is continuously embedded in $L^1(\mathbb{R}^d)$. The first one can be estimated by

$$\begin{aligned}\int_{\mathbb{R}} \sup_{|\tilde{\mathbf{r}}|\leqslant R} |\phi(\mathbf{r})|\,\mathrm{d}r_d &= \int_{\mathbb{R}} \frac{1+r_d^2}{1+r_d^2} \sup_{|\tilde{\mathbf{r}}|\leqslant R} |\phi(\mathbf{r})|\,\mathrm{d}r_d \leqslant \sup_{r_d\in\mathbb{R}}\left((1+r_d^2)\sup_{|\tilde{\mathbf{r}}|\leqslant R}|\phi(\mathbf{r})|\right)\int_{\mathbb{R}} \frac{\mathrm{d}y_d}{1+y_d^2} \\ &\leqslant C \sup_{\mathbf{r}\in\mathbb{R}^d} \left|(1+r_d^2)\phi(\mathbf{r})\right|.\end{aligned}$$

□

Lemma 3.2 *Let $d \geqslant 2$. The partial Fourier transform $\tilde{\mathcal{F}}G$ is given by the locally integrable function*

$$\tilde{\mathcal{F}}G(\mathbf{r}) = (2\pi)^{\frac{1-d}{2}} \frac{\mathrm{i}\mathrm{e}^{\mathrm{i}\kappa(\tilde{\mathbf{r}})|r_d|}}{2\kappa(\tilde{\mathbf{r}})}. \tag{3.4}$$

Proof: The d-dimensional Fourier transform $\hat{G}$ is a tempered distribution and can be expressed as

$$\langle \hat{G}, \phi\rangle = (2\pi)^{-\frac{d}{2}} \lim_{\epsilon\to 0^+} \int_{\mathbb{R}^d} \frac{\phi(\mathbf{k})}{|\mathbf{k}|^2 - k_0^2 - \mathrm{i}\epsilon}\,\mathrm{d}\mathbf{k}, \quad \phi \in \mathcal{S}(\mathbb{R}^d). \tag{3.5}$$

This formula can be derived as follows. Given $\epsilon > 0$, consider the Helmholtz operator $-\Delta - (k_0^2 + \mathrm{i}\epsilon)$. An outgoing fundamental solution of this operator is given by

$$G_\epsilon(\mathbf{r}) = \frac{\mathrm{i}}{4}\left(\frac{k}{2\pi|\mathbf{r}|}\right)^{\frac{d-2}{2}} H^{(1)}_{\frac{d-2}{2}}(k\,|\mathbf{r}|)$$

where k denotes the principal square root of $k_0^2 + \mathrm{i}\epsilon$, see [35, Chap. 9]. Since G_ϵ is a fundamental solution of $-\Delta - (k_0^2 + \mathrm{i}\epsilon)$ and a tempered distribution, its Fourier transform may be identified with the locally integrable function $\hat{G}_\epsilon(\mathbf{y}) = (2\pi)^{-d/2}(|\mathbf{y}|^2 - (k_0^2 + \mathrm{i}\epsilon))^{-1}$. Further, by using the asymptotic estimates (2.4)-(2.5), see also [11, (13)], and Lebesgue's dominated convergence theorem it can be shown that $G_\epsilon \xrightarrow{\mathcal{S}'} G$ and therefore also $\hat{G}_\epsilon \xrightarrow{\mathcal{S}'} \hat{G}$, which is (3.5).

Exploiting the fact that $\tilde{\mathcal{F}} = \mathcal{F}_d^{-1}\mathcal{F}$ we obtain

$$\langle \tilde{\mathcal{F}}G, \phi\rangle = (2\pi)^{-\frac{d}{2}} \lim_{\epsilon\to 0^+} \int_{\mathbb{R}^d} \frac{\mathcal{F}_d^{-1}\phi(\mathbf{k})}{|\mathbf{k}|^2 - k_0^2 - \mathrm{i}\epsilon}\,\mathrm{d}\mathbf{k} = (2\pi)^{-\frac{d+1}{2}} \lim_{\epsilon\to 0^+} \int_{\mathbb{R}^d}\int_{\mathbb{R}} \frac{\mathrm{e}^{\mathrm{i}r_d k_d}\phi(\tilde{\mathbf{k}}, r_d)}{|\mathbf{k}|^2 - k_0^2 - \mathrm{i}\epsilon}\,\mathrm{d}r_d\,\mathrm{d}\mathbf{k}.$$

Applying Fubini's theorem to interchange integration with respect to k_d and r_d we obtain

$$\langle \tilde{\mathcal{F}}G, \phi\rangle = (2\pi)^{-\frac{d+1}{2}} \lim_{\epsilon\to 0^+} \int_{\mathbb{R}^d} \phi(\tilde{\mathbf{k}}, r_d) \int_{\mathbb{R}} \frac{\mathrm{e}^{\mathrm{i}r_d k_d}}{|\mathbf{k}|^2 - k_0^2 - \mathrm{i}\epsilon}\,\mathrm{d}k_d\,\mathrm{d}(\tilde{\mathbf{k}}, r_d).$$

Concerning the inner integral define κ_ϵ as the square root of $\kappa^2 + \mathrm{i}\epsilon$ with positive imaginary part and use formula 17.23.14 in [17] to obtain

$$\int_{\mathbb{R}} \frac{\mathrm{e}^{\mathrm{i}r_d k_d}}{|\mathbf{k}|^2 - k_0^2 - \mathrm{i}\epsilon}\,\mathrm{d}k_d = \int_{\mathbb{R}} \frac{\mathrm{e}^{\mathrm{i}r_d k_d}}{k_d^2 - \kappa(\tilde{\mathbf{k}})^2 - \mathrm{i}\epsilon}\,\mathrm{d}k_d = \int_{\mathbb{R}} \frac{\mathrm{e}^{\mathrm{i}r_d k_d}}{k_d^2 + (-\mathrm{i}\kappa_\epsilon(\tilde{\mathbf{k}}))^2}\,\mathrm{d}k_d = \frac{\pi \mathrm{e}^{\mathrm{i}\kappa_\epsilon(\tilde{\mathbf{k}})|r_d|}}{-\mathrm{i}\kappa_\epsilon(\tilde{\mathbf{k}})}.$$

Thus, we have shown that

$$\langle \tilde{\mathcal{F}}G, \phi\rangle = (2\pi)^{\frac{1-d}{2}} \lim_{\epsilon\to 0^+} \int_{\mathbb{R}^d} \phi(\tilde{\mathbf{k}}, r_d) \frac{\mathrm{i}\mathrm{e}^{\mathrm{i}\kappa_\epsilon(\tilde{\mathbf{k}})|r_d|}}{2\kappa_\epsilon(\tilde{\mathbf{k}})}\, \mathrm{d}(\tilde{\mathbf{k}}, r_d). \tag{3.6}$$

Finally, we can interchange limit and integral by Lebesgue's dominated convergence theorem, since $|\kappa_\epsilon| > |\kappa|$ and the integrand in (3.6) is dominated by $|\phi|/|2\kappa|$, which is in $L^1(\mathbb{R}^d)$ according to Lemma 3.1. Therefore,

$$\langle \tilde{\mathcal{F}}G, \phi\rangle = (2\pi)^{\frac{1-d}{2}} \int_{\mathbb{R}^d} \phi(\tilde{\mathbf{k}}, r_d) \frac{\mathrm{i}\mathrm{e}^{\mathrm{i}\kappa(\tilde{\mathbf{k}})|r_d|}}{2\kappa(\tilde{\mathbf{k}})}\, \mathrm{d}(\tilde{\mathbf{k}}, r_d). \qquad \square$$

Having found $\tilde{\mathcal{F}}G$ we calculate $\tilde{\mathcal{F}}u$ in Theorem 3.3. For $d \geqslant 2$ define

$$\mathbf{h}^{\pm}\colon \mathbb{R}^{d-1} \to \mathbb{C}^d,\ \mathbf{h}^{\pm}(\tilde{\mathbf{r}}) := \begin{pmatrix} \tilde{\mathbf{r}} \\ \pm\kappa(\tilde{\mathbf{r}}) \end{pmatrix}. \tag{3.7}$$

We also introduce the half space

$$E_a := \{\mathbf{y} \in \mathbb{R}^d : y_d \geqslant a\}, \quad a \in \mathbb{R},$$

and the indicator function $\mathbf{1}_A$ of a set A, which is defined by $\mathbf{1}_A(x) := 1$ if $x \in A$ and $\mathbf{1}_A(x) := 0$ otherwise. Regarding the right-hand side of (3.8) below, we recall that the Fourier transform of a function with compact support in $\mathbb{R}^d$ can be extended to an entire function on $\mathbb{C}^d$.

Theorem 3.3 (Generalized Fourier Diffraction Theorem) *Let $d \geqslant 2$. Assume that $g \in L^1(\mathbb{R}^d)$ has compact support. Then $\tilde{\mathcal{F}}u$, where $u = g * G$, is given by the following locally integrable function*

$$\tilde{\mathcal{F}}u(\mathbf{r}) = \sqrt{\frac{\pi}{2}} \frac{\mathrm{i}}{\kappa(\tilde{\mathbf{r}})} \left(\mathrm{e}^{\mathrm{i}\kappa(\tilde{\mathbf{r}})r_d} \mathcal{F}\big((1 - \mathbf{1}_{E_{r_d}})g\big)(\mathbf{h}^+(\tilde{\mathbf{r}})) + \mathrm{e}^{-\mathrm{i}\kappa(\tilde{\mathbf{r}})r_d} \mathcal{F}\left(\mathbf{1}_{E_{r_d}} g\right)(\mathbf{h}^-(\tilde{\mathbf{r}}))\right), \tag{3.8}$$

for $\mathbf{r} \in \mathbb{R}^d$ with $|\tilde{\mathbf{r}}| \neq k_0$. If r_d is sufficiently large or sufficiently small such that

$$\pm(r_d - y_d) > 0 \quad \textit{for all } \mathbf{y} \in \operatorname{supp} g, \tag{3.9}$$

then (3.8) simplifies to

$$\tilde{\mathcal{F}}u(\mathbf{r}) = \sqrt{\frac{\pi}{2}}\, \frac{\mathrm{i}\mathrm{e}^{\pm\mathrm{i}\kappa(\tilde{\mathbf{r}})r_d}}{\kappa(\tilde{\mathbf{r}})} \hat{g}(\mathbf{h}^{\pm}(\tilde{\mathbf{r}})). \tag{3.10}$$

Proof: There is a compact set $K \subset \mathbb{R}^d$ and a sequence $(g_n) \subset \mathcal{D}(\mathbb{R}^d)$ converging to g in $L^1(\mathbb{R}^d)$ such that K contains the supports of g and all g_n. Define $u_n = g_n * G$. Then, in the sense of tempered distributions we have

$$\tilde{\mathcal{F}}u_n = \mathcal{F}_d^{-1}\mathcal{F}(g_n * G) = (2\pi)^{\frac{d}{2}} \mathcal{F}_d^{-1}(\hat{g}_n \hat{G}) = (2\pi)^{\frac{d-1}{2}} \tilde{\mathcal{F}}g_n \overset{d}{*} \tilde{\mathcal{F}}G,$$

the last equality being a consequence of the convolution theorem for partial Fourier transforms and $\overset{d}{*}$ denoting partial convolution along the d-th coordinate, see [28, Def. 8.21, Thm. 8.22]. Taking into account Lemma 3.2, it follows that

$$\tilde{\mathcal{F}}u_n(\mathbf{r}) = \int_{\mathbb{R}} \frac{\mathrm{i}\mathrm{e}^{\mathrm{i}\kappa(\tilde{\mathbf{r}})|r_d - y|}}{2\kappa(\tilde{\mathbf{r}})} \tilde{\mathcal{F}}g_n(\tilde{\mathbf{r}}, y)\, \mathrm{d}y$$

wherever $\kappa \neq 0$. So, for every $\phi \in \mathcal{S}(\mathbb{R}^d)$

$$\langle \tilde{\mathcal{F}}u_n, \phi\rangle = \frac{\mathrm{i}}{2} \int_{\mathbb{R}^d} \frac{\phi(\mathbf{r})}{\kappa(\tilde{\mathbf{r}})} \int_{\mathbb{R}} \mathrm{e}^{\mathrm{i}\kappa(\tilde{\mathbf{r}})|r_d - y|} \tilde{\mathcal{F}}g_n(\tilde{\mathbf{r}}, y)\, \mathrm{d}y\, \mathrm{d}\mathbf{r}. \tag{3.11}$$

Next, we rewrite the inner integral as a sum of two d-dimensional Fourier transforms.

$$\begin{aligned}
&\int_{\mathbb{R}} \mathrm{e}^{\mathrm{i}\kappa(\tilde{\mathbf{r}})|r_d-y|}\tilde{\mathcal{F}}g_n(\tilde{\mathbf{r}},y)\,\mathrm{d}y \\
&\quad= \int_{-\infty}^{r_d} \mathrm{e}^{\mathrm{i}\kappa(\tilde{\mathbf{r}})(r_d-y)}\tilde{\mathcal{F}}g_n(\tilde{\mathbf{r}},y)\,\mathrm{d}y + \int_{r_d}^{+\infty} \mathrm{e}^{\mathrm{i}\kappa(\tilde{\mathbf{r}})(y-r_d)}\tilde{\mathcal{F}}g_n(\tilde{\mathbf{r}},y)\,\mathrm{d}y \\
&\quad= \mathrm{e}^{\mathrm{i}\kappa(\tilde{\mathbf{r}})r_d}\int_{\mathbb{R}} \mathbf{1}_{(-\infty,r_d)}(y)\mathrm{e}^{-\mathrm{i}\kappa(\tilde{\mathbf{r}})y}\tilde{\mathcal{F}}g_n(\tilde{\mathbf{r}},y)\,\mathrm{d}y + \mathrm{e}^{-\mathrm{i}\kappa(\tilde{\mathbf{r}})r_d}\int_{\mathbb{R}} \mathbf{1}_{(r_d,\infty)}(y)\mathrm{e}^{\mathrm{i}\kappa(\tilde{\mathbf{r}})y}\tilde{\mathcal{F}}g_n(\tilde{\mathbf{r}},y)\,\mathrm{d}y \\
&\quad= \frac{\mathrm{e}^{\mathrm{i}\kappa(\tilde{\mathbf{r}})r_d}}{(2\pi)^{\frac{d-1}{2}}}\int_{\mathbb{R}^d} \mathbf{1}_{(-\infty,r_d)}(y)g_n(\tilde{\mathbf{x}},y)\mathrm{e}^{-\mathrm{i}(\tilde{\mathbf{x}}\cdot\tilde{\mathbf{r}}+\kappa(\tilde{\mathbf{r}})y)}\,\mathrm{d}(\tilde{\mathbf{x}},y) \\
&\qquad+ \frac{\mathrm{e}^{-\mathrm{i}\kappa(\tilde{\mathbf{r}})r_d}}{(2\pi)^{\frac{d-1}{2}}}\int_{\mathbb{R}^d} \mathbf{1}_{(r_d,\infty)}(y)g_n(\tilde{\mathbf{x}},y)\mathrm{e}^{-\mathrm{i}(\tilde{\mathbf{x}}\cdot\tilde{\mathbf{r}}-\kappa(\tilde{\mathbf{r}})y)}\,\mathrm{d}(\tilde{\mathbf{x}},y) \\
&\quad= (2\pi)^{\frac{1}{2}}\left(\mathrm{e}^{\mathrm{i}\kappa(\tilde{\mathbf{r}})r_d}\mathcal{F}\big((1-\mathbf{1}_{E_{r_d}})g_n\big)(\mathbf{h}^+(\tilde{\mathbf{r}})) + \mathrm{e}^{-\mathrm{i}\kappa(\tilde{\mathbf{r}})r_d}\mathcal{F}\big(\mathbf{1}_{E_{r_d}}g_n\big)(\mathbf{h}^-(\tilde{\mathbf{r}}))\right)
\end{aligned}$$

Therefore (3.11) equals

$$\langle\tilde{\mathcal{F}}u_n,\phi\rangle = \mathrm{i}\sqrt{\frac{\pi}{2}}\int_{\mathbb{R}^d}\frac{\phi(\mathbf{r})}{\kappa(\tilde{\mathbf{r}})}\left(\mathrm{e}^{\mathrm{i}\kappa(\tilde{\mathbf{r}})r_d}\mathcal{F}\big((1-\mathbf{1}_{E_{r_d}})g_n\big)(\mathbf{h}^+(\tilde{\mathbf{r}})) + \mathrm{e}^{-\mathrm{i}\kappa(\tilde{\mathbf{r}})r_d}\mathcal{F}\big(\mathbf{1}_{E_{r_d}}g_n\big)(\mathbf{h}^-(\tilde{\mathbf{r}}))\right)\mathrm{d}\mathbf{r}. \tag{3.12}$$

Now consider the limit $n\to\infty$ in (3.12). Regarding the left-hand side, we have $u_n\to u$ in $\mathcal{S}'(\mathbb{R}^d)$ by Theorem 2.4, since $\bigcup_n \operatorname{supp} g_n \subset K$ is bounded. Continuity of $\tilde{\mathcal{F}}$ on $\mathcal{S}'(\mathbb{R}^d)$ gives

$$\lim_{n\to\infty}\langle\tilde{\mathcal{F}}u_n,\phi\rangle = \langle\tilde{\mathcal{F}}u,\phi\rangle, \quad \text{for all } \phi\in\mathcal{S}(\mathbb{R}^d).$$

To resolve the limit on the right-hand side we use the dominated convergence theorem. The pointwise limit of the integrand is given by

$$\frac{\phi(\mathbf{r})}{\kappa(\tilde{\mathbf{r}})}\left(\mathrm{e}^{\mathrm{i}\kappa(\tilde{\mathbf{r}})r_d}\mathcal{F}\big((1-\mathbf{1}_{E_{r_d}})g\big)(\mathbf{h}^+(\tilde{\mathbf{r}})) + \mathrm{e}^{-\mathrm{i}\kappa(\tilde{\mathbf{r}})r_d}\mathcal{F}\big(\mathbf{1}_{E_{r_d}}g\big)(\mathbf{h}^-(\tilde{\mathbf{r}}))\right). \tag{3.13}$$

To see this, we note that $g_n\to g$ in $L^1(K)$ and also $\mathbf{1}_{E_{r_d}}g_n\to\mathbf{1}_{E_{r_d}}g$ in $L^1(K)$ for all $r_d\in\mathbb{R}$. Consequently, $\mathcal{F}(\mathbf{1}_{E_{r_d}}g_n)\to\mathcal{F}(\mathbf{1}_{E_{r_d}}g)$ pointwise on $\mathbb{C}^d$, cf. [20, (7.3.1)]. Hence $\mathcal{F}(\mathbf{1}_{E_{r_d}}g_n)(\mathbf{h}^-(\tilde{\mathbf{r}}))\to\mathcal{F}(\mathbf{1}_{E_{r_d}}g)(\mathbf{h}^-(\tilde{\mathbf{r}}))$ for all $\mathbf{r}\in\mathbb{R}^d$. Analogously, we find that $\mathcal{F}((1-\mathbf{1}_{E_{r_d}})g_n)(\mathbf{h}^+(\tilde{\mathbf{r}}))\to\mathcal{F}((1-\mathbf{1}_{E_{r_d}})g)(\mathbf{h}^+(\tilde{\mathbf{r}}))$ for all $\mathbf{r}\in\mathbb{R}^d$.

Next, it follows from (3.11) that the integrand is bounded by $\sqrt{2\pi}\,\|g_n\|_{L^1}\,|\phi/2\kappa|$. Since we can find a C such that $\|g_n\|_{L^1}\leqslant C\,\|g\|_{L^1}$ for all n we have found an upper bound.

Finally, it follows from the dominated convergence theorem that (3.13) is in $L^1(\mathbb{R}^d)$ and

$$\langle\tilde{\mathcal{F}}u,\phi\rangle = \mathrm{i}\sqrt{\frac{\pi}{2}}\int_{\mathbb{R}^d}\frac{\phi(\mathbf{r})}{\kappa(\tilde{\mathbf{r}})}\left(\mathrm{e}^{\mathrm{i}\kappa(\tilde{\mathbf{r}})r_d}\mathcal{F}\big((1-\mathbf{1}_{E_{r_d}})g\big)(\mathbf{h}^+(\tilde{\mathbf{r}})) + \mathrm{e}^{-\mathrm{i}\kappa(\tilde{\mathbf{r}})r_d}\mathcal{F}\big(\mathbf{1}_{E_{r_d}}g\big)(\mathbf{h}^-(\tilde{\mathbf{r}}))\right)\mathrm{d}\mathbf{r}$$

for all $\phi\in\mathcal{S}(\mathbb{R}^d)$, which proves (3.8). Furthermore, if (3.9) is fulfilled, one of the two Fourier transforms on the right-hand side of (3.8) vanishes, while the other one equals $\hat{g}$, so that we obtain (3.10), which finishes the proof. ▫

Remark 3.4 (1D Fourier diffraction theorem) Theorem 3.3 can be extended to dimension $d=1$ in the following way. Let $g\in L^1(\mathbb{R})$ be compactly supported and recall from (2.7) the simple expression of the one-dimensional fundamental solution. Then a direct calculation yields

$$u(x) = \frac{\mathrm{i}}{2k_0}\int_{\mathbb{R}} g(y)\mathrm{e}^{\mathrm{i}k_0|x-y|}\,\mathrm{d}y = \sqrt{\frac{\pi}{2}}\frac{\mathrm{i}}{k_0}\left(\mathrm{e}^{\mathrm{i}k_0x}\mathcal{F}\left((1-\mathbf{1}_{E_x})g\right)(k_0) + \mathrm{e}^{-\mathrm{i}k_0x}\mathcal{F}\left(\mathbf{1}_{E_x}g\right)(-k_0)\right).$$

If x lies outside the support of g, that is, $\pm(x-y)>0$ for all $y\in\operatorname{supp} g$, then

$$u(x) = \sqrt{\frac{\pi}{2}}\frac{\mathrm{i}}{k_0}\mathrm{e}^{\pm\mathrm{i}k_0x}\hat{g}(\pm k_0).$$

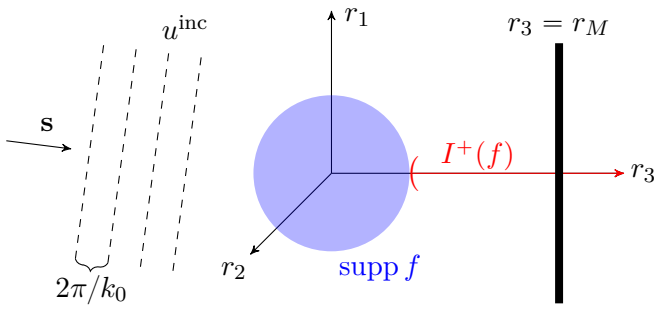

FIGURE 1. *Measurement setup for $d = 3$ with the open interval $I^+(f)$ marked in red along the r_3 axis. The incident field has direction $\mathbf{s}$ and wavelength $2\pi/k_0$.*

Remark 3.5 Since g has compact support, $\tilde{\mathcal{F}}u$ is smooth wherever $|\tilde{\mathbf{r}}| \neq k_0$ according to (3.8). On the other hand, consider $\tilde{\mathbf{r}}_0 \in \mathbb{R}^{d-1}$ with $|\tilde{\mathbf{r}}_0| = k_0$ and note that $\mathcal{F}((1 - \mathbf{1}_{E_{r_d}})g) \circ \mathbf{h}^+$ and $\mathcal{F}(\mathbf{1}_{E_{r_d}} g) \circ \mathbf{h}^-$ are continuous functions on $\mathbb{R}^{d-1}$. Evaluating the long bracket in (3.8) at $(\tilde{\mathbf{r}}_0, r_d)$ gives $\hat{g}(\tilde{\mathbf{r}}_0, 0)$ for every $r_d \in \mathbb{R}$. Thus, the function $\tilde{\mathcal{F}}u$ has a singularity at $(\tilde{\mathbf{r}}_0, r_d)$, for every $r_d \in \mathbb{R}$, if $\hat{g}(\tilde{\mathbf{r}}_0, 0) \neq 0$.

4. FOURIER COVERAGE

In this section we investigate some of the ramifications of Theorem 3.3 for data collection strategies in diffraction tomography. Therefore, we return to the inverse scattering problem outlined in Section 1. Under the Born or Rytov approximation, cf. (1.5) and (1.6), the governing equation is

$$-(\Delta + k_0^2)u(\mathbf{r}) = k_0^2 f(\mathbf{r}) u^{\text{inc}}(\mathbf{r}), \quad \mathbf{r} \in \mathbb{R}^d, \tag{4.1}$$

where u^{inc} is the incident wave and the outgoing solution u approximates the scattered wave. The normalized scattering potential f, recall (1.4), is the unknown we aim to reconstruct. From now on we impose the following assumptions, which are standard in diffraction tomography.

(i) The incident field is a plane wave $u^{\text{inc}}(\mathbf{r}) = \mathrm{e}^{\mathrm{i}k_0 \mathbf{s}\cdot\mathbf{r}}$ for some $\mathbf{s} \in \mathbb{S}^{d-1}$.

(ii) The measurement hyperplane $\{\mathbf{r} \in \mathbb{R}^d : r_d = r_{\text{M}}\}$ is disjoint from $\operatorname{supp} f$, i.e. condition (3.9) holds. Introducing the intervals

$$I^{\pm} = I^{\pm}(f) = \{x \in \mathbb{R} : x \gtrless y_d \text{ for all } \mathbf{y} \in \operatorname{supp} f\}, \tag{4.2}$$

this condition can be written as $r_{\text{M}} \in I^{\pm}$.

Figure 1 illustrates the measurement setup. The following d-dimensional version of the Fourier diffraction theorem, see also [21, 38, 48], is now an immediate consequence of Theorem 3.3. Recall the partial Fourier transform $\tilde{\mathcal{F}}$ in (3.1), κ in (3.2) and $\mathbf{h}$ in (3.7).

Corollary 4.1 (Fourier diffraction theorem) *Let $d \geqslant 2$ and assume that $f \in L^1(\mathbb{R}^d)$ has compact support. Then, for $\mathbf{x} \in \mathbb{R}^{d-1}$ with $|\mathbf{x}| \neq k_0$, the outgoing solution u of (4.1) satisfies*

$$\tilde{\mathcal{F}}u(\mathbf{x}, r_{\text{M}}) = \sqrt{\frac{\pi}{2}} \frac{\mathrm{i}\mathrm{e}^{\pm \mathrm{i}\kappa(\mathbf{x}) r_{\text{M}}} k_0^2}{\kappa(\mathbf{x})} \hat{f}(\mathbf{h}^{\pm}(\mathbf{x}) - k_0 \mathbf{s}), \qquad \text{if } r_{\text{M}} \in I^{\pm}(f). \tag{4.3}$$

Remark 4.2 (Variants of the Fourier diffraction theorem) In the present article, the main application of Theorem 3.3 is the special case Corollary 4.1 based on assumptions *(i)* and *(ii)*. On the other hand, it is precisely the absence of these assumptions which makes Theorem 3.3 more general and potentially more widely applicable. That is, Theorem 3.3 could be used in situations, where the data are collected on a hyperplane passing through the inhomogeneity or where the incident field u^{inc} is not a plane wave. Consider, for instance, an incident Herglotz wave

$$u^{\mathrm{inc}}(\mathbf{r}) = \int_{\mathbb{S}^{d-1}} a(\mathbf{s}) \mathrm{e}^{\mathrm{i}k_0 \mathbf{s}\cdot\mathbf{r}} \,\mathrm{d}s(\mathbf{s}),$$

where $a \in L^2(\mathbb{S}^{d-1})$. Replacing g in (3.10) with $k_0^2 f u^{\mathrm{inc}}$ and changing the order of integration yields

$$\tilde{\mathcal{F}}u(\mathbf{x}, r_{\mathrm{M}}) = \sqrt{\frac{\pi}{2}} \frac{\mathrm{i}\mathrm{e}^{\pm \mathrm{i}\kappa(\mathbf{x}) r_{\mathrm{M}}} k_0^2}{\kappa(\mathbf{x})} \int_{\mathbb{S}^{d-1}} a(\mathbf{s}) \hat{f}(\mathbf{h}^{\pm}(\mathbf{x}) - k_0 \mathbf{s}) \,\mathrm{d}s(\mathbf{s}).$$

Such relations between $\tilde{\mathcal{F}}u$ and $\hat{f}$ have recently been used for tomographic reconstructions in [27]. Moreover, we note that the applicability of Theorem 3.3 is not restricted to outgoing solutions: Suppose w is an arbitrary solution of (2.1). Then $w = u + v$, where u is the outgoing solution and $\Delta v + k_0^2 v = 0$ on $\mathbb{R}^d$. If $\tilde{\mathcal{F}}v$ can be calculated, then $\tilde{\mathcal{F}}w = \tilde{\mathcal{F}}u + \tilde{\mathcal{F}}v$ and, using Theorem 3.3, one obtains a formula for $\tilde{\mathcal{F}}w$. Finally, we remark that there are vector-valued versions of the Fourier diffraction theorem, see [30, 36].

So far all parameters of the experiment were kept fixed. In that case the Fourier diffraction theorem in (4.3) gives information about $\mathcal{F}f$ on the hemisphere

$$\{\mathbf{h}^{\pm}(\mathbf{x}) - k_0 \mathbf{s} : \mathbf{x} \in \mathbb{R}^{d-1}, \, |\mathbf{x}| < k_0\} \tag{4.4}$$

with center $-k_0\mathbf{s}$ and radius k_0. This is called the *Fourier coverage* or *k-space coverage* of the experiment and we denote it by $\mathcal{Y} \subset \mathbb{R}^d$. The restriction $|\mathbf{x}| < k_0$ is made for the practical reason that the larger spatial frequencies do not contribute to the physical measurements.

The set in (4.4), however, is only a null set. For a viable reconstruction, we need to obtain more information, namely a larger Fourier coverage, by adapting the experimental setup. In this section, we discuss how altering

(i) the direction of incidence $\mathbf{s}$,

(ii) the orientation and position of the object,

(iii) the orientation and position of the measurement hyperplane, or

(iv) the wave number k_0

affects the Fourier coverage $\mathcal{Y}$. Regarding the first three constituents, the decisive factor is their orientation *relative to each other*. A change in one of them is equivalent to a corresponding change in the other two. For instance, measurements obtained from rotating the object during illumination can be reproduced, at least theoretically, by rotating the direction of incidence and the measurement equipment in a corresponding fashion. Altering the wave number k_0 is different in character and will be treated in Section 4.4. Finally, as a preparation for the general filtered backpropagation presented in Section 5, we consider in Section 4.5 an experiment where all the above constituents may vary simultaneously.

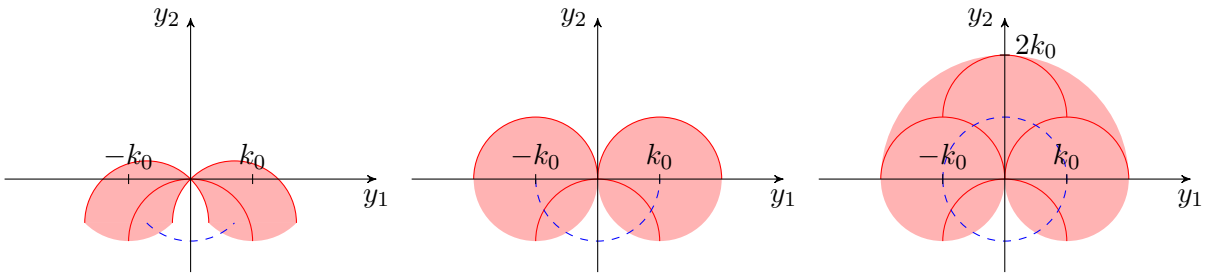

FIGURE 2. *2D Fourier coverage for incidence direction varying according to* $\mathbf{s}(t) = (\cos t, \sin t)$ *where* $t \in [\pi/4, 3\pi/4]$ *(left),* $t \in [0, \pi]$ *(center) and* $t \in [0, 2\pi]$ *(right). Measurements are taken at* $r_2 = r_{\mathrm{M}}$ *with* $r_{\mathrm{M}} \in I^+$*, recall (4.2). The Fourier coverage (light red) is a union of infinitely many semicircles, some of which are depicted in red. Their centers lie on the dashed blue curve.*

4.1. Direction of incidence. Altering the incidence direction $\mathbf{s}$ is known as *angle scanning* [31] or illumination scanning [40]. Then instead of (4.3), we obtain for $\mathbf{x} \in \mathbb{R}^{d-1}$

$$\tilde{\mathcal{F}} u_t(\mathbf{x}, r_{\mathrm{M}}) = \sqrt{\frac{\pi}{2}} \frac{\mathrm{i} \mathrm{e}^{\pm \mathrm{i}\kappa r_{\mathrm{M}}} k_0^2}{\kappa} \mathcal{F} f\left(\mathbf{h}^{\pm} - k_0 \mathbf{s}(t)\right), \qquad \text{if } r_{\mathrm{M}} \in I^{\pm}, \tag{4.5}$$

where u_t, $0 \leqslant t \leqslant L$, is the scattered wave generated by the incident plane wave $\mathbf{r} \mapsto \mathrm{e}^{\mathrm{i}k_0 \mathbf{r} \cdot \mathbf{s}(t)}$ and $\mathbf{s} \colon [0, L] \to \mathbb{S}^{d-1}$ is the varying direction of incidence. Thus the Fourier coverage is given by

$$\mathcal{Y} = \left\{ \mathbf{h}^{\pm}(\mathbf{x}) - k_0 \mathbf{s}(t) \in \mathbb{R}^d : |\mathbf{x}| < k_0,\ 0 \leqslant t \leqslant L \right\}.$$

Geometrically speaking, it consists of translations of the semicircle or hemisphere (4.4) such that its center stays at a distance of k_0 from the origin, see Figure 2.

4.2. Rigid motion of object. If the object moves according to a rigid motion $(t, \mathbf{r}) \mapsto R(t)^{\top} \mathbf{r} + \mathbf{d}(t)$ with a rotation matrix

$$R(t) \in SO(d) := \{ Q \in \mathbb{R}^{d \times d} : Q^{\top} Q = I,\ \det Q = 1 \}$$

and a translation vector $\mathbf{d}(t) \in \mathbb{R}^d$, $t \in [0, L]$, it has the normalized scattering potential $f \circ \Psi_t$ with

$$\Psi_t \colon \mathbb{R}^d \to \mathbb{R}^d, \quad \mathbf{r} \mapsto R(t)(\mathbf{r} - \mathbf{d}(t)). \tag{4.6}$$

We denote by $u_t = k_0^2((f \circ \Psi_t) u^{\mathrm{inc}}) * G$ the wave scattered by this transformed potential and assume that $r_{\mathrm{M}} \in I^{\pm}(f \circ \Psi_t)$ for all $t \in [0, L]$. Then (4.3) becomes

$$\tilde{\mathcal{F}} u_t(\mathbf{x}, r_{\mathrm{M}}) = \sqrt{\frac{\pi}{2}} \frac{\mathrm{i} \mathrm{e}^{\pm \mathrm{i}\kappa r_{\mathrm{M}}} k_0^2}{\kappa} \mathcal{F} f\left(R(t)\left(\mathbf{h}^{\pm} - k_0 \mathbf{s}\right)\right) \mathrm{e}^{-\mathrm{i}\mathbf{d}(t) \cdot (\mathbf{h}^{\pm} - k_0 \mathbf{s})}, \tag{4.7}$$

cf. [42, sect. 2.2]. In this case we obtain the Fourier coverage

$$\mathcal{Y} = \left\{ R(t)\left(\mathbf{h}^{\pm}(\mathbf{x}) - k_0 \mathbf{s}\right) \in \mathbb{R}^d : |\mathbf{x}| < k_0,\ 0 \leqslant t \leqslant L \right\},$$

which depends only on the rotation R but not on the translation $\mathbf{d}$. It consists of rotated versions of the semicircle or hemisphere from (4.4), see Figure 3, Figure 4 and Figure 5. Comparing with Figure 2 shows that rotating the object is not equivalent to rotating the incidence in terms of Fourier coverage.

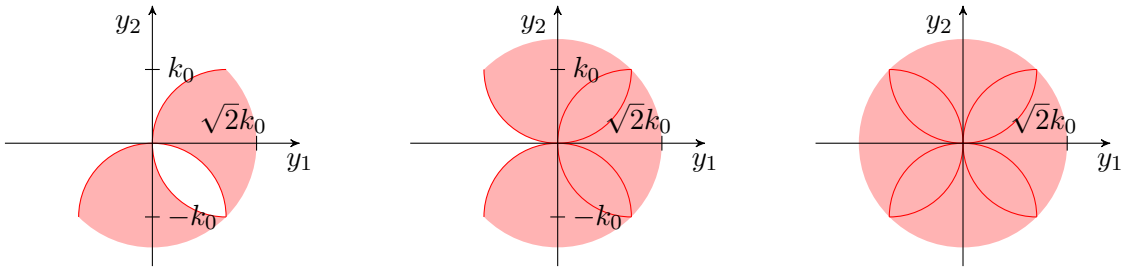

(a) *Quarter turn* (b) *Half turn* (c) *Full turn*

FIGURE 3. *2D Fourier coverage for a rotating object, incidence direction* $\mathbf{s} = (0, 1)$ *and measurements taken at* $r_2 = r_{\mathrm{M}} \in I^+$. *The Fourier coverage (light red) is a union of infinitely many semicircles, some of which are depicted in red.*

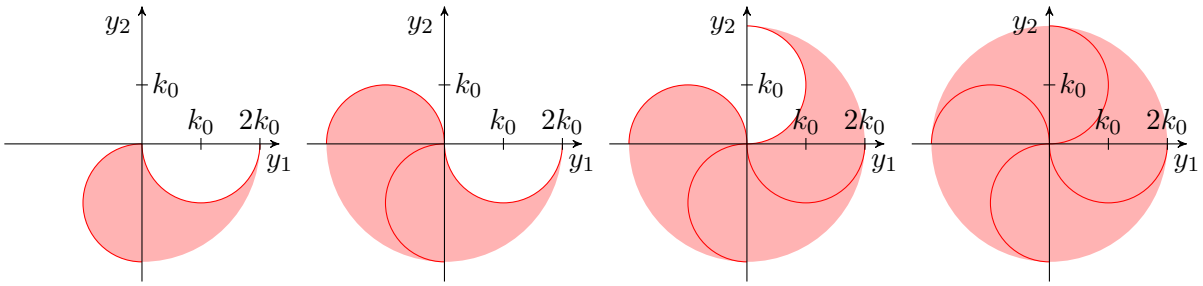

(a) *Quarter turn* (b) *Half turn* (c) *Three-quarter turn* (d) *Full turn*

FIGURE 4. *2D Fourier coverage for a rotating object, incidence direction* $\mathbf{s} = (1, 0)$ *and measurements taken at* $r_2 = r_{\mathrm{M}} \in I^+$. *The Fourier coverage (light red) is a union of infinitely many semicircles, some of which are depicted in red.*

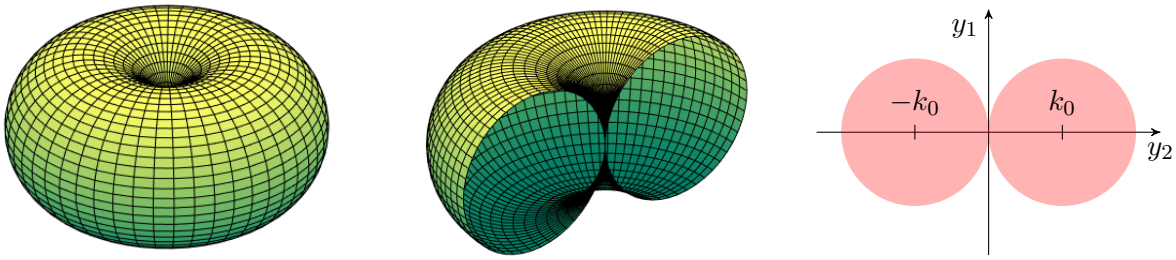

FIGURE 5. *3D Fourier coverage for a full rotation of the object about the* r_1*-axis with incidence direction* $\mathbf{s} = (0, 1, 0)$. Left and center: *3D visualization.* Right: *2D cross section through* y_1y_2*-plane. In this case there is no difference in the Fourier coverage between* $r_{\mathrm{M}} \in I^+$ *or* $r_{\mathrm{M}} \in I^-$.

4.3. Location of measurement hyperplane. Consider now moving the measurement hyperplane. It follows from (4.3) that the signed distance r_{M} from the origin to the hyperplane does not affect the Fourier coverage, at least as long as it stays on one side of the support of f. Therefore, we keep r_{M} fixed and rotate the measurement hyperplane around the origin according to $R(t) \in SO(d)$. This is equivalent to rotating the incidence direction and the object simultaneously. Denote by $\mathbf{s}_0$ the original incidence direction. Combining (4.5) for the incidence $\mathbf{s}(t) = R(t)^\top \mathbf{s}_0$ with (4.7) for the normalized scattering potential $f(R(t)\cdot)$, we obtain

$$\begin{aligned}\tilde{\mathcal{F}} u_t(\mathbf{x}, r_{\mathrm{M}}) &= \sqrt{\frac{\pi}{2}} \frac{\mathrm{i} e^{\pm \mathrm{i}\kappa r_{\mathrm{M}}}}{\kappa} \mathcal{F} f\left(R(t)\left(\mathbf{h}^\pm(\mathbf{x}) - k_0 R(t)^\top \mathbf{s}_0\right)\right) \\ &= \sqrt{\frac{\pi}{2}} \frac{\mathrm{i} e^{\pm \mathrm{i}\kappa r_{\mathrm{M}}}}{\kappa} \mathcal{F} f\left(R(t)\mathbf{h}^\pm(\mathbf{x}) - k_0 \mathbf{s}_0\right), \qquad \text{if } r_{\mathrm{M}} \in I^\pm(f \circ R(t)).\end{aligned}$$

The resulting Fourier coverage is

$$\mathcal{Y} = \left\{ R(t)\mathbf{h}^{\pm}(\mathbf{x}) - k_0\mathbf{s}_0 \in \mathbb{R}^d : |\mathbf{x}| < k_0,\ 0 \leqslant t \leqslant L \right\}.$$

The hemisphere $\mathbf{h}^{\pm}$, which is centered at the origin, is rotated *before* it is translated by the fixed vector $-k_0\mathbf{s}_0$. This means that $\mathcal{Y} \subset \{\mathbf{y} \in \mathbb{R}^d : |\mathbf{y} - k_0\mathbf{s}_0| = k_0\}$. In contrast to the previous two situations, the coverage is always a set of measure zero. See Figure 6.

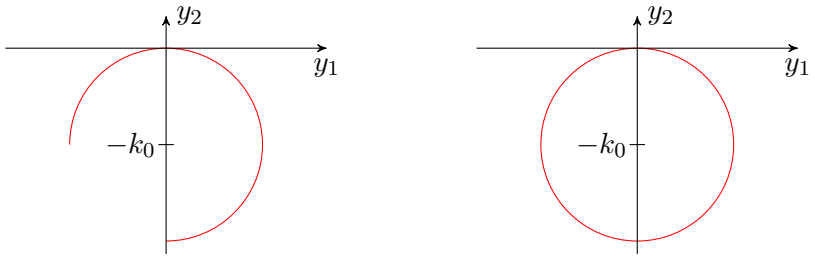

FIGURE 6. *2D Fourier coverage for rotating measurement line, starting with the measurement line $r_2 = r_{\mathrm{M}} \in I^+$ and rotating it clockwise. Left: Quarter turn. Right: Half turn (or more). Note that the coverage is only the circle, not its interior.*

4.4. Wave number. We examine how altering the wave number k_0 of the incident plane wave affects the Fourier coverage. Denote by u_t the scattered wave generated by the incident field $u^{\mathrm{inc}}(\mathbf{x}) = \mathrm{e}^{\mathrm{i}k_0(t)\,\mathbf{x}\cdot\mathbf{s}}$ with wave number $k_0(t) > 0$ for $t \in [0, L]$. We assume that the object's refractive index n and therefore also f does not depend on $k_0(t)$. Then, according to (4.3), we have

$$\tilde{\mathcal{F}}u_t(\mathbf{x}, r_{\mathrm{M}}) = \sqrt{\frac{\pi}{2}}\frac{\mathrm{i}\mathrm{e}^{\pm\mathrm{i}\kappa(\mathbf{x},t)r_{\mathrm{M}}}k_0(t)^2}{\kappa(\mathbf{x},t)}\mathcal{F}f\left(\mathbf{h}^{\pm}(\mathbf{x},t) - k_0(t)\mathbf{s}\right), \qquad \text{if } r_{\mathrm{M}} \in I^{\pm}.$$

Notice that $\kappa(\mathbf{x},t) = \sqrt{k_0(t)^2 - |\mathbf{x}|^2}$ and therefore also $\mathbf{h}^{\pm}(\mathbf{x},t) = (\mathbf{x}, \pm\kappa(\mathbf{x},t))^{\top}$ depend on t in this case. The Fourier coverage

$$\mathcal{Y} = \left\{ \mathbf{h}^{\pm}(\mathbf{x},t) - k_0(t)\mathbf{s} \in \mathbb{R}^d : 0 \leqslant t \leqslant L,\ |\mathbf{x}| < k_0(t) \right\}$$

is a union of hemispheres that are translated in direction of $\mathbf{s}$ and scaled such that each passes through the origin. In contrast to the previous scenarios, there are large missing parts near the origin, see the 2D case in Figure 7. This also holds in 3D, where the corresponding Fourier coverages are obtained by rotating those depicted in Figure 7 around the y_2 axis.

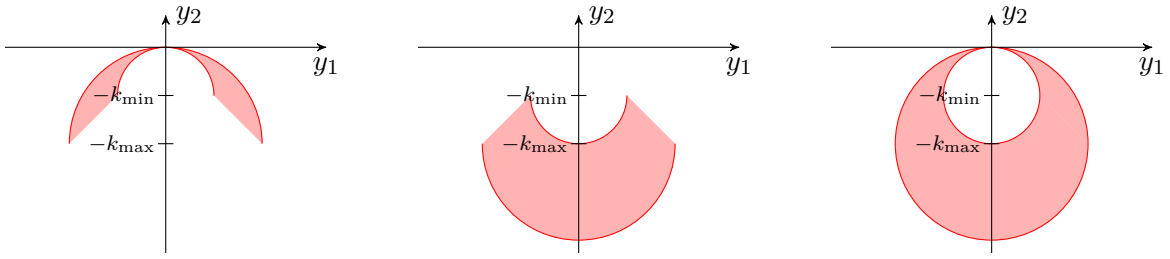

FIGURE 7. *2D Fourier coverage with $\mathbf{s} = (0, 1)$ where the wave number $k_0(t)$ covers the interval $[k_{\min}, k_{\max}]$. Left: measurements taken at $r_2 = r_{\mathrm{M}}$ with $r_{\mathrm{M}} \in I^+$. Center: $r_{\mathrm{M}} \in I^-$. Right: both measurements combined.*

4.5. Varying all parameters at once. Let us assume that the object rotation $R(t) \in SO(d)$, the translation $\mathbf{d}(t) \in \mathbb{R}^d$, the incidence direction $\mathbf{s}(t) \in \mathbb{S}^{d-1}$ and the wave number $k_0(t) \in \mathbb{R}_{>0}$ all depend on $t \in [0, L]$. We denote by $u_t^{\mathrm{inc}}(\mathbf{r}) = \mathrm{e}^{\mathrm{i}k_0(t)\mathbf{r}\cdot\mathbf{s}(t)}$ the corresponding incident wave and by

$$u_t := k_0(t)^2 \left((f \circ \Psi_t)\, u_t^{\mathrm{inc}} \right) * G \tag{4.8}$$

the resulting wave scattered by $f \circ \Psi_t$, see (4.6). Analogously to (4.7), we have

$$\tilde{\mathcal{F}} u_t(\mathbf{x}, r_{\mathrm{M}}) = \sqrt{\frac{\pi}{2}} \frac{\mathrm{i}\mathrm{e}^{\pm \mathrm{i}\kappa(\mathbf{x},t) r_{\mathrm{M}}}\, k_0(t)^2}{\kappa(\mathbf{x},t)} \mathcal{F} f \left(R(t) \left(\mathbf{h}^{\pm}(\mathbf{x},t) - k_0(t)\mathbf{s}(t) \right) \right) \mathrm{e}^{-\mathrm{i}\mathbf{d}(t)\cdot\left(\mathbf{h}^{\pm}(\mathbf{x},t) - k_0(t)\mathbf{s}(t)\right)} \tag{4.9}$$

if $r_{\mathrm{M}} \in I^{\pm}(f \circ \Psi_t)$, and the respective Fourier coverage is given by

$$\mathcal{Y} = \left\{ R(t) \left(\mathbf{h}^{\pm}(\mathbf{x},t) - k_0(t)\, \mathbf{s}(t) \right) \in \mathbb{R}^d : |\mathbf{x}| < k_0(t),\, 0 \leqslant t \leqslant L \right\}.$$

Remark 4.3 (Maximal cover) Assume that $k_0(t)$ has a maximum $k_{\max}$. Then, under the assumptions of Section 4.5 the set $\mathcal{Y}$ is always contained in a ball of radius $2k_{\max}$. In 2D this maximal coverage can be attained when the object makes a full turn and the propagation direction of the plane wave is parallel to the measurement line, see Figure 4d. On the other hand, the fact that $\mathcal{Y}$ is bounded while $\operatorname{supp} \hat{f}$ is unbounded implies that f cannot be reconstructed exactly using the Fourier diffraction theorem alone [48].

Remark 4.4 (Redundancy of measurement planes) So far we have always considered two options for the location of the measurement hyperplane, $r_{\mathrm{M}} \in I^-$ or $r_{\mathrm{M}} \in I^+$, each leading to a different coverage in general. The following argument shows that all information obtained at one hyperplane can also be obtained at the other by suitably adapting the incidence direction and the orientation of the object. For instance, the frequency components of f obtained at I^- (and thus via $\mathbf{h}^-$) can be accessed at I^+ (and via $\mathbf{h}^+$) when replacing the incidence $\mathbf{s}_0 = (s_1, \dots, s_d) \in \mathbb{S}^{d-1}$ by $(s_1, \dots, s_{d-2}, -s_{d-1}, -s_d)$ and using the rotation $R_0 = \operatorname{diag}(1, \dots, 1, -1, -1) \in SO(d)$, since we have for $\mathbf{x} \in \mathbb{R}^{d-1}$ with $|\mathbf{x}| < k_0$ that

$$\mathbf{h}^+(\mathbf{x}) - k_0 \mathbf{s}_0 = R_0 \big(\mathbf{h}^-(x_1, \dots, x_{d-2}, -x_{d-1}) - k_0(s_1, \dots, s_{d-2}, -s_{d-1}, -s_d) \big).$$

5. Filtered backpropagation

Filtered backpropagation formulae provide an explicit expression for a low-pass filtered approximation of the normalized scattering potential f, see [9], [21, Sect. 6.4.2] or [28]. Recall the Fourier coverage $\mathcal{Y} \subset \mathbb{R}^d$ of the experiment from the previous section. The filtered backpropagation of f is defined by the Fourier inversion

$$f_{\mathcal{Y}} := \mathcal{F}^{-1}(\mathbf{1}_{\mathcal{Y}} \hat{f}).$$

If $\hat{f}$ is integrable on $\mathcal{Y}$, we can express the filtered backpropagation by the integral

$$f_{\mathcal{Y}}(\mathbf{r}) = (2\pi)^{-\frac{d}{2}} \int_{\mathcal{Y}} \hat{f}(\mathbf{y}) \mathrm{e}^{\mathrm{i}\mathbf{y}\cdot\mathbf{r}}\, \mathrm{d}\mathbf{y}. \tag{5.1}$$

Before applying the Fourier diffraction theorem, Corollary 4.1, to express the right-hand side in terms of the measurements $u_t(\cdot, r_{\mathrm{M}})$, the integral is typically transformed into one over $(\mathbf{x}, t)$. Recall that $\mathbf{x} = (x_1, \dots, x_{d-1})$ are the spatial frequencies of the measurements of the scattered wave. This change of coordinates circumvents the irregular sampling in the Fourier domain, which would result from directly discretizing (4.9).

The following characterization of the filtered backpropagation is a direct consequence of Plancherel's identity, which states that $\|f\|_{L^2(\mathbb{R}^d)} = \|\hat{f}\|_{L^2(\mathbb{R}^d)}$ for all $f \in L^2(\mathbb{R}^d)$.

Theorem 5.1 *Let $f \in L^2(\mathbb{R}^d)$ and the Fourier coverage $\mathcal{Y} \subset \mathbb{R}^d$ be measurable. Then*

(i) $f_{\mathcal{Y}}$ has minimal L^2 norm among all functions $g \in L^2(\mathbb{R}^d)$ that satisfy $\hat{g} = \hat{f}$ on $\mathcal{Y}$,

(ii) $f_{\mathcal{Y}}$ is the L^2 best approximation to f in the subspace $\{g \in L^2(\mathbb{R}^d) : \operatorname{supp} \hat{g} \subset \mathcal{Y}\}$, and

(iii) if $\mathcal{Y}_1 \supset \mathcal{Y}$, then $\|f - f_{\mathcal{Y}_1}\|_{L^2(\mathbb{R}^d)} \leqslant \|f - f_{\mathcal{Y}}\|_{L^2(\mathbb{R}^d)}$.

5.1. General filtered backpropagation formula. We consider the general experiment of Section 4.5 in which the direction of incidence $\mathbf{s}(t) \in \mathbb{S}^{d-1}$, the object orientation $R(t) \in SO(d)$ and translation $\mathbf{d}(t) \in \mathbb{R}^d$, as well as the wave number $k_0(t) > 0$ can vary simultaneously depending on $t \in [0, L]$. As pointed out in Remark 4.4, we can restrict ourselves to a measurement hyperplane with $r_{\mathrm{M}} \in I^+$ without losing generality. Therefore, we set accordingly $\mathbf{h} := \mathbf{h}^+$, see (3.7), and define

$$\mathcal{U} := \Big\{(\mathbf{x}, t) \in \mathbb{R}^d : |\mathbf{x}| < k_0(t), 0 \leqslant t \leqslant L\Big\}. \tag{5.2}$$

The Fourier coverage of the experiment is given by $\mathcal{Y} = T(\mathcal{U})$, where

$$T \colon \mathcal{U} \to \mathbb{R}^d, \quad T(\mathbf{x}, t) := R(t)(\mathbf{h}(\mathbf{x}, t) - k_0(t)\mathbf{s}(t)). \tag{5.3}$$

With this notation, we obtain by (4.9) the following relation between the scattered wave u_t and the normalized scattering potential f,

$$\tilde{\mathcal{F}} u_t(\mathbf{x}, r_{\mathrm{M}}) = \sqrt{\frac{\pi}{2}} \frac{\mathrm{i} \mathrm{e}^{\mathrm{i}\kappa r_{\mathrm{M}}}\, k_0(t)^2}{\kappa}\, \mathcal{F} f(T(\mathbf{x}, t))\, \mathrm{e}^{-\mathrm{i}\mathbf{d}(t)\cdot T(\mathbf{x},t)}. \tag{5.4}$$

Remark 5.2 (Experimental setup with discontinuous parameters) The following backpropagation formula in Theorem 5.4 specifically allows $\mathbf{s}$, R and k_0 to be discontinuous functions of t. This was done in order to be able to handle experimental setups where one or more of those parameters do not change continuously but only attain a few discrete values, without having to impose unrealistic smoothness assumptions. Imagine, for instance, an object which is subsequently rotated about two different axes, or, one which, during rotation, is subsequently illuminated from a finite number of directions. Such situations can be modeled by a piecewise smooth rotation map R or a piecewise constant $\mathbf{s}$, respectively. Subsequently, all obtained measurements can be combined into one reconstruction using equation (5.7) below.

For proving the filtered backpropagation formula, we need the following change of variables formula, which is due to [19, Thm. 2], see also [4, Thm. 5.8.30]. The quantity $\operatorname{Card}(T^{-1}(\mathbf{y}))$ is called the *Banach indicatrix* of the map T, where Card denotes the counting measure.

Lemma 5.3 *Let $\Omega \subset \mathbb{R}^d$ be an open set and let $T \colon \Omega \to \mathbb{R}^d$ be a measurable map that has partial derivatives a.e. in Ω. Denote by $\det(\nabla T)$ the determinant of the matrix formed by the partial derivatives of T. Suppose, in addition, that T has the Luzin N property, which means that T maps null sets to null sets. Then, for every measurable set $\mathcal{E} \subset \Omega$ and every measurable function $v \colon \mathbb{R}^d \to \mathbb{R}$, the functions*

$$v(T(\mathbf{r}))\, |\det(\nabla T(\mathbf{r}))|\, \mathbf{1}_{\mathcal{E}}(\mathbf{r}) \quad \text{and} \quad v(\mathbf{y})\, \operatorname{Card}(T^{-1}(\mathbf{y}) \cap \mathcal{E}) \tag{5.5}$$

are measurable, where we set $v(T(\mathbf{r}))\, |\det \nabla T(\mathbf{r})| = 0$ if $v(T(\mathbf{r}))$ is not defined. If one of these functions is integrable, then so is the other and

$$\int_{\mathcal{E}} v(T(\mathbf{r}))\, |\det(\nabla T(\mathbf{r}))|\, \mathrm{d}\mathbf{r} = \int_{\mathbb{R}^d} v(\mathbf{y})\, \operatorname{Card}(T^{-1}(\mathbf{y}) \cap \mathcal{E})\, \mathrm{d}\mathbf{y}. \tag{5.6}$$

Theorem 5.4 (Filtered backpropagation formula) *Let $f \in L^1(\mathbb{R}^d)$ have compact support and $L > 0$. Assume that each of the maps $\mathbf{s}\colon [0,L] \to \mathbb{S}^{d-1}$, $R\colon [0,L] \to SO(d)$, $\mathbf{d}\colon [0,L] \to \mathbb{R}^d$ and $k_0\colon [0,L] \to (0,+\infty)$ is piecewise C^1 in every component, i.e., except at finitely many points $t_1, \dots, t_m \in [0,L]$, and that $\mathbf{s}'$, R', and k_0' are bounded. Let u_t be defined as in (4.8) and assume that $r_{\mathrm{M}} \in I^+(f \circ \Psi_t)$ for all $t \in [0,L]$. Then, $f_{\mathcal{Y}}(\mathbf{r})$ is finite for all $\mathbf{r} \in \mathbb{R}^d$ and*

$$f_{\mathcal{Y}}(\mathbf{r}) = 2(2\pi)^{-\frac{1+d}{2}} \int_{\mathcal{U}} \frac{\kappa(\mathbf{x},t)\, \mathrm{e}^{\mathrm{i}T(\mathbf{x},t)\cdot(\mathbf{r}+\mathbf{d}(t))}\, \tilde{\mathcal{F}} u_t(\mathbf{x}, r_{\mathrm{M}})\, |\det(\nabla T(\mathbf{x},t))|}{k_0(t)^2\, \mathrm{ie}^{\mathrm{i}\kappa(\mathbf{x},t) r_{\mathrm{M}}}\, \mathrm{Card}(T^{-1}(T(\mathbf{x},t)))}\, \mathrm{d}(\mathbf{x},t), \tag{5.7}$$

where the Jacobian determinant of T, as defined in (5.3), is given by

$$\det(\nabla T(\mathbf{x},t)) = \frac{k_0(t)k_0'(t) - R(t)\mathbf{h}(\mathbf{x},t) \cdot (k_0(t)R(t)\mathbf{s}(t))'}{\kappa(\mathbf{x},t)}. \tag{5.8}$$

Proof: We note that

$$|T(\mathbf{x},t)| \leqslant 2 \sup\{k_0(t) : t \in [0,L]\}$$

for all $(\mathbf{x},t) \in \mathcal{U}$, cf. Remark 4.3. As k_0' and therefore k_0 is bounded, the set $\mathcal{Y}$ is bounded. Therefore, $f_{\mathcal{Y}}(\mathbf{r})$ is finite for every $\mathbf{r} \in \mathbb{R}^d$. We will prove the theorem through usage of the change of variables formula in Lemma 5.3 with $\Omega = \mathbb{R}^d$, $\mathcal{E} = \mathcal{U}$ and $v = \mathbf{1}_{T(\mathcal{U})}$. To this end, we need to show that T from (5.3) fulfills the prerequisites of Lemma 5.3. By assumption, T has partial derivatives a.e. on $\mathcal{U}$, and we set T to zero on $\mathbb{R}^d \backslash \mathcal{U}$ to obtain this property on whole $\Omega = \mathbb{R}^d$. According to [44, Lem. 7.25], differentiable maps from $\mathbb{R}^d$ into $\mathbb{R}^d$ have the Luzin N property. Now let $\mathcal{L}$ denote the d-dimensional Lebesgue measure and consider $E \subset \mathcal{U}$ with $\mathcal{L}(E) = 0$. Let $D = \{(\mathbf{x},t) \in \mathcal{U} : t \in \{0, t_1, \dots, t_m, L\}\}$ be the set where T might not be C^1. By decomposing $E = (E \cap D) \cup (E \cap D^{\mathrm{c}})$ with D^{c} being the complement of D in $\mathcal{U}$, we obtain

$$\begin{aligned}\mathcal{L}(T(E)) &= \mathcal{L}(T((E \cap D) \cup (E \cap D^{\mathrm{c}}))) = \mathcal{L}(T(E \cap D) \cup T(E \cap D^{\mathrm{c}})) \\ &\leqslant \mathcal{L}(T(E \cap D)) + \mathcal{L}(T(E \cap D^{\mathrm{c}})) \leqslant \mathcal{L}(T(D)) + \mathcal{L}(T(E \cap D^{\mathrm{c}})) = 0\end{aligned}$$

as $T(D)$ is a finite union of hypersurfaces, recall (4.4), and T is C^1 on D^{c}. Therefore, T has the Luzin N property.

Next we show that the left-hand side of (5.5) is integrable, which is equivalent to $\det(\nabla T) \in L^1(\mathcal{U})$. For almost every $t \in [0,L]$ the Jacobian matrix of T is given by

$$\nabla T = \begin{pmatrix} \frac{\partial T}{\partial x_1} & \cdots & \frac{\partial T}{\partial x_{d-1}} & \frac{\partial T}{\partial t} \end{pmatrix},$$

where

$$\begin{aligned}\frac{\partial T}{\partial k_i} &= R\frac{\partial \mathbf{h}}{\partial x_i} = R\left(\mathbf{e}_i - \frac{x_i}{\kappa}\mathbf{e}_d\right), \\ \frac{\partial T}{\partial t} &= R\frac{\partial \mathbf{h}}{\partial t} + R'\mathbf{h} - (k_0 R\mathbf{s})' = \frac{k_0 k_0'}{\kappa} R\mathbf{e}_d + R'\mathbf{h} - (k_0 R\mathbf{s})'\end{aligned}$$

and $\mathbf{e}_i$ denotes the i-th unit vector in $\mathbb{R}^d$. Therefore, its determinant can be expressed as

$$\det(\nabla T) = \det\left(R^{\top}\nabla T\right) = \det\left(\begin{array}{c|c} I_{d-1} & \frac{k_0 k_0'}{\kappa}\mathbf{e}_d + \mathbf{v} \\ -\mathbf{x}^{\top}/\kappa & \end{array}\right) = \frac{k_0 k_0'}{\kappa} + \det\left(\begin{array}{c|c} I_{d-1} & \mathbf{v} \\ -\mathbf{x}^{\top}/\kappa & \end{array}\right),$$

where I_{d-1} is the identity matrix of size $d-1$ and $\mathbf{v} = R^{\top}(R'\mathbf{h} - (k_0 R\mathbf{s})')$. For the determinant of a 2×2 block matrix with invertible upper left block we recall that

$$\det\begin{pmatrix} A & B \\ C & D \end{pmatrix} = \det\left(\begin{pmatrix} A & 0 \\ C & I \end{pmatrix}\begin{pmatrix} I & A^{-1}B \\ 0 & D - CA^{-1}B \end{pmatrix}\right) = \det(A)\det(D - CA^{-1}B).$$

It follows that

$$\det\left(\begin{array}{c|c} I_{d-1} & \mathbf{v} \\ -\mathbf{x}^\top/\kappa & \end{array}\right) = v_d - \frac{\mathbf{x}^\top \overline{\mathbf{v}}}{-\kappa} = \frac{\mathbf{h}\cdot\mathbf{v}}{\kappa}.$$

In total the Jacobian determinant equals

$$\det(\nabla T) = \frac{k_0 k_0' + \mathbf{h}\cdot\mathbf{v}}{\kappa}.$$

Due to the stated assumptions on k_0, R and $\mathbf{s}$ the numerator is bounded. Therefore, the determinant is integrable on $\mathcal{U}$, if $1/\kappa$ is. Recalling (3.3), we see that

$$\begin{aligned}\left\|\frac{1}{\kappa}\right\|_{L^1(\mathcal{U})} = \int_{\mathcal{U}} \frac{\mathrm{d}(\mathbf{x},t)}{|\kappa|} &\leqslant \left|\mathbb{S}^{d-2}\right| \int_0^L k_0(t)^{d-\frac{5}{2}} \int_0^{k_0(t)} \frac{\mathrm{d}\rho}{\sqrt{|k_0(t)-\rho|}}\,\mathrm{d}t \\ &= 2\left|\mathbb{S}^{d-2}\right| \int_0^L k_0(t)^{d-2}\,\mathrm{d}t,\end{aligned}$$

which is finite since k_0 is bounded. We conclude that the assumptions of Lemma 5.3 are fulfilled and in particular (5.6) with $\mathcal{E} = \mathcal{U}$ and $v = \mathbf{1}_{T(\mathcal{U})}$ yields

$$\int_{T(\mathcal{U})} \mathrm{Card}(T^{-1}(\mathbf{y}))\,\mathrm{d}\mathbf{y} = \int_{\mathcal{U}} |\det(\nabla T(\mathbf{x},t))|\,\mathrm{d}(\mathbf{x},t).$$

Therefore, $\mathrm{Card}(T^{-1}(\mathbf{y})) < \infty$ for a.e. $\mathbf{y} \in T(\mathcal{U})$. As $\mathrm{Card}(T^{-1}(\cdot)) > 0$ on $T(\mathcal{U})$, we may then write

$$f_{\mathcal{Y}}(\mathbf{r}) = (2\pi)^{-\frac{d}{2}} \int_{T(\mathcal{U})} \mathrm{e}^{\mathrm{i}\mathbf{y}\cdot\mathbf{r}} \mathcal{F}f(\mathbf{y}) \frac{\mathrm{Card}(T^{-1}(\mathbf{y}))}{\mathrm{Card}(T^{-1}(\mathbf{y}))}\,\mathrm{d}\mathbf{y}.$$

Invoking Lemma 5.3 again, where we now integrate the function

$$v(\mathbf{y}) = \begin{cases} \mathrm{e}^{\mathrm{i}\mathbf{y}\cdot\mathbf{r}} \mathcal{F}f(\mathbf{y}) / \mathrm{Card}(T^{-1}(\mathbf{y})), & \mathbf{y} \in T(\mathcal{U}), \\ 0, & \text{otherwise}, \end{cases}$$

gives

$$f_{\mathcal{Y}}(\mathbf{r}) = (2\pi)^{-\frac{d}{2}} \int_{\mathcal{U}} \mathrm{e}^{\mathrm{i}T(\mathbf{x},t)\cdot\mathbf{r}} \mathcal{F}f(T(\mathbf{x},t)) \frac{|\det(\nabla T(\mathbf{x},t))|}{\mathrm{Card}(T^{-1}(T(\mathbf{x},t)))}\,\mathrm{d}(\mathbf{x},t). \tag{5.9}$$

By (5.4), we can express $\mathcal{F}f$ in terms of the measurements and (5.7) is then established.

It remains to verify (5.8). We have already shown that

$$\det(\nabla T) = \frac{k_0 k_0' + \mathbf{h}\cdot\left(R^\top(R'\mathbf{h} - (k_0 R\mathbf{s})')\right)}{\kappa}.$$

In order to finish the calculation, we only have to observe that the matrix $R^\top R'$ is skew-symmetric, which can be seen by differentiating the identity $R^\top R = I_d$. Therefore, $\mathbf{y}\cdot R^\top R'\mathbf{y} = 0$ for all $\mathbf{y} \in \mathbb{R}^d$. □

5.2. Non-absorbing object. In many situations, such as optical diffraction tomography of biological cells, the refractive index n and therefore the normalized scattering potential f are assumed to be real-valued, which means that absorption is neglected, cf. [2, 37]. Then the Fourier transform of $f\colon \mathbb{R}^d \to \mathbb{R}$ is conjugate symmetric,

$$\mathcal{F}f(\mathbf{y}) = \overline{\mathcal{F}f(-\mathbf{y})}, \qquad \forall \mathbf{y} \in \mathbb{R}^d, \tag{5.10}$$

also known as Friedel's law, where $\overline{z}$ denotes the complex conjugate of $z \in \mathbb{C}$. The reconstruction $f_{\mathcal{Y}}$ does not account for this symmetry. It might even happen that $f_{\mathcal{Y}}$ has a non-vanishing imaginary part despite the fact that f is real-valued.

By (5.10), we obtain from the measurements the Fourier transform $\mathcal{F}f$ not only on $\mathcal{Y}$, but also on $-\mathcal{Y} = \{-\mathbf{y} : \mathbf{y} \in \mathcal{Y}\}$, and therefore the extended Fourier coverage

$$\mathcal{Y}_{\mathrm{sym}} := \mathcal{Y} \cup (-\mathcal{Y}). \tag{5.11}$$

Analogously to Theorem 5.1, the backpropagation $f_{\mathcal{Y}_{\mathrm{sym}}}$ minimizes $\|g\|_{L^2(\mathbb{R}^d)}$ among all real-valued functions $g \in L^2(\mathbb{R}^d)$ that satisfy $\mathcal{F}g = \mathcal{F}f$ on $\mathcal{Y}$. In order to provide a backpropagation formula for $f_{\mathcal{Y}_{\mathrm{sym}}}$ similar to (5.7), we set

$$\mathcal{U}_{\mathrm{sym}} := \Big\{(\mathbf{x}, t) \in \mathbb{R}^d : |\mathbf{x}| < k_0(|t|), -L \leqslant t \leqslant L\Big\},$$

and we replace the coordinate transformation T of (5.3) by

$$T_{\mathrm{sym}} \colon \mathcal{U}_{\mathrm{sym}} \to \mathbb{R}^d, \quad T_{\mathrm{sym}}(\mathbf{x}, t) := \operatorname{sgn}(t)\, T(\mathbf{x}, |t|), \tag{5.12}$$

with the sign function

$$\operatorname{sgn}(t) := \begin{cases} \frac{t}{|t|}, & t \neq 0, \\ 0, & t = 0. \end{cases} \tag{5.13}$$

Here, a negative t is associated with the reflected points $-T_{\mathrm{sym}}(\mathbf{x}, -t)$ in Fourier space.

Theorem 5.5 (Filtered backpropagation with non-absorbing object) *Let the assumptions of Theorem 5.4 be satisfied. In addition, assume that f is real-valued. Then*

$$f_{\mathcal{Y}_{\mathrm{sym}}}(\mathbf{r}) = 4(2\pi)^{-\frac{d+1}{2}} \operatorname{Re}\left(\int_{\mathcal{U}} \frac{\kappa\, \mathrm{e}^{\mathrm{i}T(\mathbf{x},t)\cdot(\mathbf{r}+\mathbf{d})}\, |\det(\nabla T(\mathbf{x}, t))|\, \tilde{\mathcal{F}} u_t(\mathbf{x}, r_{\mathrm{M}})}{k_0(t)^2\, \mathrm{i}\mathrm{e}^{\mathrm{i}\kappa r_{\mathrm{M}}}\, \operatorname{Card}(T_{\mathrm{sym}}^{-1}(T(\mathbf{x}, t)))}\, \mathrm{d}(\mathbf{x}, t)\right), \tag{5.14}$$

where Re *denotes the real part, u_t is given in (4.8), and* $\det(\nabla T)$ *in (5.8).*

Proof: Since T_{sym} satisfies the same assumptions as T in the proof of Theorem 5.4 with the points of possible non-smoothness $\{-t_m, \dots, -t_1, 0, t_1, \dots, t_m\}$, we obtain analogously to the derivation of (5.9) in the proof of Theorem 5.4 that

$$f_{\mathcal{Y}_{\mathrm{sym}}}(\mathbf{r}) = (2\pi)^{-\frac{d}{2}} \int_{\mathcal{U}_{\mathrm{sym}}} \mathrm{e}^{\mathrm{i}T_{\mathrm{sym}}(\mathbf{x},t)\cdot\mathbf{r}} \mathcal{F}f(T_{\mathrm{sym}}(\mathbf{x}, t)) \frac{|\det(\nabla T_{\mathrm{sym}}(\mathbf{x}, t))|}{\operatorname{Card}(T_{\mathrm{sym}}^{-1}(T_{\mathrm{sym}}(\mathbf{x}, t)))}\, \mathrm{d}(\mathbf{x}, t).$$

Splitting up the domain of integration $\mathcal{U}_{\mathrm{sym}} = \mathcal{U} \cup \{(\mathbf{x}, t) : |\mathbf{x}| < k_0(|t|), t \in [-L, 0]\}$, we obtain

$$\begin{aligned} f_{\mathcal{Y}_{\mathrm{sym}}}(\mathbf{r}) = {} & (2\pi)^{-\frac{d}{2}} \int_{\mathcal{U}} \mathrm{e}^{\mathrm{i}T(\mathbf{x},t)\cdot\mathbf{r}} \mathcal{F}f(T(\mathbf{x}, t)) \frac{|\det(\nabla T(\mathbf{x}, t))|}{\operatorname{Card}(T_{\mathrm{sym}}^{-1}(T(\mathbf{x}, t)))}\, \mathrm{d}(\mathbf{x}, t) \\ & + (2\pi)^{-\frac{d}{2}} \int_{\mathcal{U}} \mathrm{e}^{-\mathrm{i}T(\mathbf{x},t)\cdot\mathbf{r}} \mathcal{F}f(-T(\mathbf{x}, t)) \frac{|\det(\nabla T(\mathbf{x}, t))|}{\operatorname{Card}(T_{\mathrm{sym}}^{-1}(-T(\mathbf{x}, t)))}\, \mathrm{d}(\mathbf{x}, t), \end{aligned}$$

where we have used the substitution $t \mapsto -t$ and the property $T_{\mathrm{sym}}(\mathbf{x}, -t) = -T_{\mathrm{sym}}(\mathbf{x}, t)$ in the second integral. This property also implies that $T_{\mathrm{sym}}^{-1}(\mathbf{y})$ is isomorphic to $T_{\mathrm{sym}}^{-1}(-\mathbf{y})$ and therefore $\operatorname{Card}(T_{\mathrm{sym}}^{-1}(\mathbf{y})) = \operatorname{Card}(T_{\mathrm{sym}}^{-1}(-\mathbf{y}))$ for every $\mathbf{y}$. It now follows from (5.10) that the second integral is the complex conjugate of the first so that

$$f_{\mathcal{Y}_{\mathrm{sym}}}(\mathbf{r}) = 2(2\pi)^{-\frac{d}{2}} \operatorname{Re}\left(\int_{\mathcal{U}} \mathrm{e}^{\mathrm{i}T(\mathbf{x},t)\cdot\mathbf{r}} \mathcal{F}f(T(\mathbf{x}, t)) \frac{|\det(\nabla T(\mathbf{x}, t))|}{\operatorname{Card}(T_{\mathrm{sym}}^{-1}(T(\mathbf{x}, t)))}\, \mathrm{d}(\mathbf{x}, t)\right).$$

Using the Fourier diffraction theorem in (5.4) finishes the proof. ▫

Remark 5.6 (Comparison of the backpropagation formulae) The filtered backpropagation formula with symmetrization (5.14) differs from (5.7) in that we take twice the real part and we compute the Banach indicatrix of T_{sym}. For real-valued f, we can compare the two reconstructions $f_{\mathcal{Y}_{\mathrm{sym}}}$ and $f_{\mathcal{Y}}$. By Theorem 5.1, we always have $\|f - f_{\mathcal{Y}_{\mathrm{sym}}}\|_{L^2(\mathbb{R}^d)} \leqslant \|f - f_{\mathcal{Y}}\|_{L^2(\mathbb{R}^d)}$. If $\mathcal{Y}$ is point symmetric with respect to the origin, i.e. $\mathcal{Y} = -\mathcal{Y}$, then both yield the same result. Otherwise, $f_{\mathcal{Y}}$ might have a non-vanishing imaginary part, but even considering only the real part is not ideal. In the extreme case where $\mathcal{Y} \cap (-\mathcal{Y})$ is a null set, as in Figure 4b, we obtain $f_{\mathcal{Y}_{\mathrm{sym}}} = 2\operatorname{Re}(f_{\mathcal{Y}})$, so the reconstruction with (5.14) is considerably better.

5.3. Filtered backpropagation with multi-dimensional parameter set. For 3D angle scanning, cf. Section 4.1, one option is to move the incidence along a two-dimensional set. In order to handle such an experiment, we extend the filtered backpropagation of Theorem 5.4 by making $t \in [0, L]$ a multi-dimensional parameter $\mathbf{t} \in \mathcal{A} \subset \mathbb{R}^{q+1}$ with $q \in \mathbb{N}$. We substitute $\mathbf{x} \in \mathcal{B}_{k_0}^{d-1}$ by $\mathbf{v} = \frac{\mathbf{x}}{|\mathbf{x}|} \arcsin \frac{|\mathbf{x}|}{k_0} \in \mathcal{B}_{\pi/2}^{d-1}$ if $\mathbf{x} \neq \mathbf{0}$. Then we have $\mathbf{x} = k_0 \frac{\mathbf{v}}{|\mathbf{v}|} \sin|\mathbf{v}|$ and $\kappa = k_0 \cos|\mathbf{v}|$. Accordingly, we replace the transformation T in (5.3) by

$$U \colon \mathcal{B}_{\pi/2}^{d-1} \times \mathcal{A} \to \mathbb{R}^d, \quad U(\mathbf{v}, \mathbf{t}) := k_0(\mathbf{t})\, R(\mathbf{t}) \left(\begin{pmatrix} \mathbf{v} \frac{\sin|\mathbf{v}|}{|\mathbf{v}|} \\ \cos|\mathbf{v}| \end{pmatrix} - \mathbf{s}(\mathbf{t}) \right).$$

This parameter change makes U Lipschitz, as opposed to T. For a set $S \subset \mathbb{R}^{d+q}$, we define $\operatorname{diam}(S) := \sup\{|\mathbf{u} - \mathbf{v}| : \mathbf{u}, \mathbf{v} \in S\}$ and the q-dimensional Hausdorff measure

$$H^q(S) := \sup_{\delta > 0} \left(\inf \left\{ \sum_{i=1}^{\infty} \frac{\pi^{q/2} \operatorname{diam}(B_i)^q}{\Gamma(\frac{q}{2} + 1)\, 2^q} : \bigcup_{i=1}^{\infty} B_i \supset S,\ B_i \subset \mathbb{R}^{d+q},\ \operatorname{diam}(B_i) < \delta \right\} \right).$$

Theorem 5.7 *Let $\mathcal{A} \subset \mathbb{R}^{q+1}$ be a bounded, open set and each of the maps $R \colon \mathcal{A} \to SO(d)$, $\mathbf{s} \colon \mathcal{A} \to \mathbb{S}^{d-1}$, $\mathbf{d} \colon \mathcal{A} \to \mathbb{R}^d$, and $k_0 \colon \mathcal{A} \to (0, +\infty)$ be C^1 with bounded partial derivatives. Further let $f \in L^1(\mathbb{R}^d)$ have compact support, $u_{\mathbf{t}}$ be defined as in (4.8) and $r_{\mathrm{M}} \in I^+(f \circ \Psi_{\mathbf{t}})$ for all $\mathbf{t} \in \mathcal{A}$. Denote by $|\nabla U|$ the square root of the sum of the squares of the determinants of the $d \times d$ minors of the Jacobian of U. With $\mathcal{W} := \{\mathbf{z} \in \mathbb{R}^d : H^q(U^{-1}(\mathbf{z})) > 0\}$, we have for all $\mathbf{r} \in \mathbb{R}^d$*

$$f_{\mathcal{W}}(\mathbf{r}) = 2(2\pi)^{-\frac{d+1}{2}} \int_{\mathcal{B}_{\pi/2}^{d-1} \times \mathcal{A}} \frac{\cos|\mathbf{v}|\ \mathrm{e}^{\mathrm{i}U(\mathbf{v},\mathbf{t}) \cdot (\mathbf{r} + \mathbf{d}(\mathbf{t}))} \tilde{\mathcal{F}} u_{\mathbf{t}}(\mathbf{v} \frac{\sin|\mathbf{v}|}{|\mathbf{v}|}, r_{\mathrm{M}})\, |\nabla U(\mathbf{v}, \mathbf{t})|}{\mathrm{i}\mathrm{e}^{\mathrm{i}k_0(\mathbf{t}) r_{\mathrm{M}} \cos|\mathbf{v}|}\, k_0(\mathbf{t})\, H^q(U^{-1}(U(\mathbf{v}, \mathbf{t})))} \,\mathrm{d}(\mathbf{v}, \mathbf{t}).$$

Proof: We first show that U is Lipschitz. All partial derivatives of U with respect to $\mathbf{t}$ are bounded by assumption. Since $|\mathbf{v}|^{-1} \sin|\mathbf{v}| \leqslant 1$ for all $\mathbf{v} \in \mathbb{R}^{d-1} \backslash \{\mathbf{0}\}$, we see that

$$\frac{\partial U(\mathbf{v}, \mathbf{t})}{\partial v_j} = k_0 R(\mathbf{t}) \begin{pmatrix} \frac{\sin|\mathbf{v}|}{|\mathbf{v}|} \mathbf{e}^j + \mathbf{v} \frac{v_j}{|\mathbf{v}|} \left(\frac{\cos|\mathbf{v}|}{|\mathbf{v}|} - \frac{\sin|\mathbf{v}|}{|\mathbf{v}|^2} \right) \\ -\frac{\mathbf{v}}{|\mathbf{v}|} \sin|\mathbf{v}| \end{pmatrix}, \qquad \forall j = 1, \ldots, d-1,$$

is uniformly bounded, which implies that U is Lipschitz. The coarea formula [14, Thm. 3.2.12], see also [34], states for any $g \in L^1(\mathcal{B}_{\pi/2}^{d-1} \times \mathcal{A})$ and Lipschitz-continuous U that

$$\int_{\mathcal{B}_{\pi/2}^{d-1} \times \mathcal{A}} g(\mathbf{v}, \mathbf{t})\, |\nabla U(\mathbf{v}, \mathbf{t})|\, \mathrm{d}(\mathbf{v}, \mathbf{t}) = \int_{\mathbb{R}^d} \int_{U^{-1}(\mathbf{z})} g(\mathbf{v}, \mathbf{t})\, \mathrm{d}H^q(\mathbf{v}, \mathbf{t})\, \mathrm{d}\mathbf{z}. \tag{5.15}$$

Plugging into (5.15) the indicator function of some $A \subset \mathcal{B}_{\pi/2}^{d-1} \times \mathcal{A}$ with $H^q(U^{-1}(U(A))) = 0$ yields $\int_A |\nabla U(\mathbf{v}, \mathbf{t})|\, \mathrm{d}(\mathbf{v}, \mathbf{t}) = 0$, and therefore $|\nabla U|$ vanishes a.e. on A. Hence (5.15) remains valid when the left integral is restricted to $S_0 := \operatorname{supp}(H^q(U^{-1} \circ U))$.

Let $\varepsilon > 0$. We define the set $S_\varepsilon := \{(\mathbf{v}, \mathbf{t}) \in \mathcal{B}_{\pi/2}^{d-1} \times \mathcal{A} : H^q(U^{-1}(U(\mathbf{v}, \mathbf{t}))) > \varepsilon\}$ and the function

$$g_\varepsilon(\mathbf{v}, \mathbf{t}) := \begin{cases} \dfrac{1}{H^q(U^{-1}(U(\mathbf{v}, \mathbf{t})))}, & (\mathbf{v}, \mathbf{t}) \in S_\varepsilon, \\ 0, & \text{otherwise}, \end{cases}$$

which is integrable on $\mathcal{B}_{\pi/2}^{d-1} \times \mathcal{A}$. Inserting g_ε into the coarea formula (5.15) yields

$$\begin{aligned} \int_{\mathcal{B}_{\pi/2}^{d-1} \times \mathcal{A}} g_\varepsilon(\mathbf{v}, \mathbf{t}) |\nabla U(\mathbf{v}, \mathbf{t})|\, \mathrm{d}(\mathbf{v}, \mathbf{t}) &= \int_{\mathbb{R}^d} \int_{U^{-1}(\mathbf{z})} g_\varepsilon(\mathbf{v}, \mathbf{t})\, \mathrm{d}H^q(\mathbf{v}, \mathbf{t})\, \mathrm{d}\mathbf{z} \\ &\leqslant \int_{\mathcal{W}} \frac{1}{H^q(U^{-1}(\mathbf{z}))} \int_{U^{-1}(\mathbf{z})} \mathrm{d}H^q(\mathbf{v}, \mathbf{t})\, \mathrm{d}\mathbf{z} \leqslant \left| \mathcal{B}_{2k_{\max}}^d \right| \end{aligned}$$

because $\mathcal{W} \subset \mathcal{B}_{2k_{\max}}^d$ by Remark 4.3. Since the right-hand side is bounded independently of ε, we see that $|\nabla U| / H^q(U^{-1} \circ U)$ is integrable on $\bigcup_{\varepsilon > 0} S_\varepsilon = S_0$.

Let $\mathbf{r} \in \mathbb{R}^d$. Then

$$a_\varepsilon(\mathbf{v},\mathbf{t}) := \mathrm{e}^{\mathrm{i}U(\mathbf{v},\mathbf{t})\cdot\mathbf{r}}\mathcal{F}f(U(\mathbf{v},\mathbf{t}))g_\varepsilon(\mathbf{v},\mathbf{t}),$$

is in $L^1(\mathcal{B}^{d-1}_{\pi/2}\times\mathcal{A})$ because $\mathcal{F}f$ is bounded. Defining $\mathcal{W}_\varepsilon := U^{-1}(S_\varepsilon)$ and inserting a_ε into (5.15), we obtain

$$\begin{aligned}\int_{S_0} a_\varepsilon(\mathbf{v},\mathbf{t})\,|\nabla U(\mathbf{v},\mathbf{t})|\,\mathrm{d}(\mathbf{v},\mathbf{t}) &= \int_{\mathcal{W}} \frac{\mathrm{e}^{\mathrm{i}\mathbf{z}\cdot\mathbf{r}}\mathcal{F}f(\mathbf{z})}{H^q(U^{-1}(\mathbf{z}))}\mathbf{1}_{\mathcal{W}_\varepsilon}(\mathbf{z})\int_{U^{-1}(\mathbf{z})}\mathrm{d}H^q(\mathbf{v},\mathbf{t})\,\mathrm{d}\mathbf{z}\\ &= \int_{\mathcal{W}} \mathrm{e}^{\mathrm{i}\mathbf{z}\cdot\mathbf{r}}\mathcal{F}f(\mathbf{z})\mathbf{1}_{\mathcal{W}_\varepsilon}(\mathbf{z})\,\mathrm{d}\mathbf{z}.\end{aligned}$$

The integrand on the left has the integrable upper bound $|\mathcal{F}f|\,|\nabla U|/H^q(U^{-1}\circ U)$, and the integrand on the right is bounded by $|\mathcal{F}f|$. Applying Lebesgue's dominated convergence theorem for $\varepsilon\to 0$ on both sides yields

$$\int_{S_0}\frac{\mathrm{e}^{\mathrm{i}U(\mathbf{v},\mathbf{t})\cdot\mathbf{r}}\mathcal{F}f(U(\mathbf{v},\mathbf{t}))}{H^q(U^{-1}(U(\mathbf{v},\mathbf{t})))}\,|\nabla U(\mathbf{v},\mathbf{t})|\,\mathrm{d}(\mathbf{v},\mathbf{t}) = \int_{\mathcal{W}}\mathrm{e}^{\mathrm{i}\mathbf{z}\cdot\mathbf{r}}\mathcal{F}f(\mathbf{z})\,\mathrm{d}\mathbf{z}.$$

Together with (4.9) and $\kappa = k_0(\mathbf{t})\cos|\mathbf{v}|$, this shows the assertion. ▫

Remark 5.8 The backpropagation formula of Theorem 5.4, if all the parameters are C^1, can be seen as a special case of Theorem 5.7. We note that for $q=0$, the set $\mathcal{W}$ coincides with $\mathcal{Y}$, while for $q\geqslant 1$ we only know the inclusion $\mathcal{W}\subset\mathcal{Y}$. Furthermore, Theorem 5.7 requires a different parameterization of the Fourier cover $\mathcal{Y}$.

5.4. Special cases. Below we give a few examples of the filtered backpropagation formulae provided by Theorem 5.4 and Theorem 5.5.

Example 5.9 (Object rotation in 2D) Consider the 2D transmission setup with incidence direction $\mathbf{s}=(0,1)^\top$, measurement line $r_2 = r_\mathrm{M}\in I^+$ and fixed wave number k_0. Assuming that the object makes a full turn according to

$$R(t) = \begin{pmatrix}\cos t & -\sin t\\ \sin t & \cos t\end{pmatrix}, \qquad t\in[0,2\pi],$$

the filtered backpropagation formula (5.7) reduces to the well-known

$$f_{\mathcal{B}_{\sqrt{2}k_0}}(\mathbf{r}) = \frac{-\mathrm{i}}{k_0}(2\pi)^{-3/2}\int_0^{2\pi}\int_{-k_0}^{k_0}\mathrm{e}^{\mathrm{i}T(x,t)\cdot\mathbf{r}-\mathrm{i}\kappa r_\mathrm{M}}\mathcal{F}_1 u_t(x,r_\mathrm{M})\,|x|\,\mathrm{d}x\,\mathrm{d}t, \qquad \text{for all } \mathbf{r}\in\mathbb{R}^2. \quad (5.16)$$

See also [9, 21, 45]. The Fourier coverage of this experiment is a disk of radius $\sqrt{2}k_0$ as depicted in Figure 3c.

Changing the incidence direction to $\mathbf{s}=(1,0)^\top$ leads to a disk of radius $2k_0$, cf. Figure 4d. This is the largest possible coverage for the given wave number, as discussed in Remark 4.3. The resulting reconstruction

$$f_{\mathcal{B}_{2k_0}}(\mathbf{r}) = \frac{-2\mathrm{i}}{k_0}(2\pi)^{-3/2}\int_0^{2\pi}\int_{-k_0}^{k_0}\mathrm{e}^{\mathrm{i}T(x,t)\cdot\mathbf{r}-\mathrm{i}\kappa r_\mathrm{M}}\mathcal{F}_1 u_t(x,r_\mathrm{M})\kappa\,\mathrm{d}x\,\mathrm{d}t, \qquad \text{for all } \mathbf{r}\in\mathbb{R}^2,$$

has a smaller L^2 approximation error than the one given in (5.16) according to Theorem 5.1.

If f is real-valued, then a half turn of the object is actually enough to recover $f_{\mathcal{B}_{2k_0}}$. This is due to Friedel's law (5.10) and the fact that the coverage $\mathcal{Y}$ for a half turn, corresponding to $t\in[0,\pi]$, see Figure 4b, satisfies $\mathcal{Y}_\mathrm{sym} = \mathcal{Y}\cup(-\mathcal{Y}) = \mathcal{B}_{2k_0}$. The symmetrized backpropagation formula from Theorem 5.5 gives

$$f_{\mathcal{B}_{2k_0}}(\mathbf{r}) = \frac{-4}{k_0}(2\pi)^{-3/2}\,\mathrm{Re}\left(\int_0^{\pi}\int_{-k_0}^{k_0}-\mathrm{i}\mathrm{e}^{\mathrm{i}T(x,t)\cdot\mathbf{r}-\mathrm{i}\kappa r_\mathrm{M}}\mathcal{F}_1 u_t(x,r_\mathrm{M})\kappa\,\mathrm{d}x\,\mathrm{d}t\right), \qquad \text{for all } \mathbf{r}\in\mathbb{R}^2.$$

Example 5.10 (2D angle scan) Consider an experimental setup of angle scanning as in Figure 2 center, which is repeated for the object rotated by 90°. With the measurement line $r_2 = r_M \in I^+$ and wave number k_0, we set the incidence $\mathbf{s}(t) = (\cos t, \sin t)$ for $t \in [0, 2\pi]$ and the piecewise constant rotation $R(t) = \pm I$ if $t \gtrless \pi$. Up to zero sets, the Fourier coverage is the union of four disks of radius k_0, namely

$$\mathcal{Y} = \mathcal{B}^2_{k_0}\left(\begin{smallmatrix} 0 \\ k_0 \end{smallmatrix}\right) \cup \mathcal{B}^2_{k_0}\left(\begin{smallmatrix} 0 \\ -k_0 \end{smallmatrix}\right) \cup \mathcal{B}^2_{k_0}\left(\begin{smallmatrix} k_0 \\ 0 \end{smallmatrix}\right) \cup \mathcal{B}^2_{k_0}\left(\begin{smallmatrix} -k_0 \\ 0 \end{smallmatrix}\right).$$

Any point in $\mathcal{Y}$ is contained either in one or in two of these disks, therefore the Banach indicatrix is given for almost every $\mathbf{y} \in \mathcal{Y}$ by

$$\operatorname{Card}(T^{-1}(\mathbf{y})) = \begin{cases} 2, & \text{if } k_0 - \sqrt{k_0^2 - y_1^2} < |y_2| < \sqrt{k_0^2 - (|y_1| - k_0)^2}, \\ 1, & \text{otherwise,} \end{cases}$$

see Figure 8 left. The backpropagation formula (5.7) becomes

$$f_{\mathcal{Y}}(\mathbf{r}) = \frac{-2\mathrm{i}(2\pi)^{-\frac{3}{2}}}{k_0} \int_0^{2\pi} \int_{-k_0}^{k_0} \frac{\mathrm{e}^{\mathrm{i}T(x,t)\cdot\mathbf{r} - \mathrm{i}\kappa(x) r_M} \mathcal{F}_1 u_t(x, r_M)}{\operatorname{Card}(T^{-1}(T(x,t)))} \, |\kappa(x)\cos t - x \sin t| \, \mathrm{d}x \, \mathrm{d}t.$$

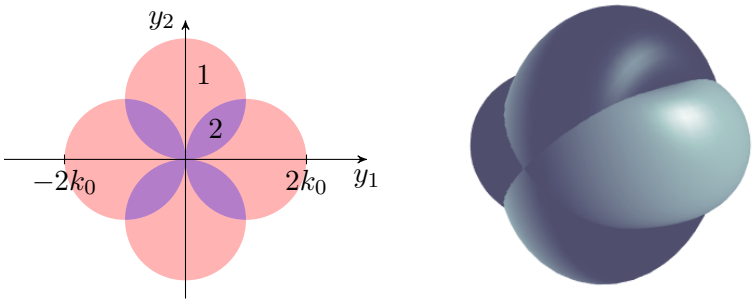

FIGURE 8. Left: *2D Fourier coverage for Example 5.10. In the purple area, the Banach indicatrix is 2, in the red area it is 1.* Right: *3D Fourier coverage for Example 5.11.*

Example 5.11 (Object rotation in 3D) We consider an experiment similar to Example 5.9 but in $\mathbb{R}^3$. The object rotates around the r_1-axis, the wave number k_0 is fixed and $r_M \in I^+$. The incidence direction $\mathbf{s} = (0, 0, 1)^\top$ leads to Devaney's filtered backpropagation formula [9]. An illustration of the Fourier coverage for this setup can be found in [28, Fig. 3].

As in $\mathbb{R}^2$, choosing $\mathbf{s} = (0, 1, 0)^\top$, i.e. parallel to the measurement plane, yields a larger coverage, cf. Figure 5. In contrast to the 2D setting, however, the Fourier coverage is considerably smaller than the maximal one. In particular, it suffers from the missing cone problem. In this case the missing regions around the origin can be filled, for instance, by subsequently rotating the object around the r_2-axis while illuminating in direction $\mathbf{s} = (1, 0, 0)^\top$. The resulting coverage $\mathcal{Y}$ is a union of two solid horn tori, one radially symmetric about the r_1-axis and the other radially symmetric about the r_2-axis, see Figure 8 right. The filtered backpropagation formula reads

$$f_{\mathcal{Y}}(\mathbf{r}) = -\frac{\mathrm{i}}{2\pi^2 k_0} \int_0^{4\pi} \int_{\mathcal{B}_{k_0}} \frac{\kappa \mathrm{e}^{\mathrm{i}T(\mathbf{x},t)\cdot\mathbf{r} - \mathrm{i}\kappa r_M} \tilde{\mathcal{F}} u_t(\mathbf{x}, r_M)}{\operatorname{Card}\left(T^{-1}(T(\mathbf{x},t))\right)} \, \mathrm{d}\mathbf{x} \, \mathrm{d}t \qquad \text{for all } \mathbf{r} \in \mathbb{R}^3,$$

where T is defined according to (5.3) with $\mathbf{s}(t) = (0, 1, 0)^\top$ for $t \in [0, 2\pi]$ and $\mathbf{s}(t) = (1, 0, 0)^\top$ for $t \in (2\pi, 4\pi]$ and the rotation matrix

$$R(t) = \begin{cases} \begin{pmatrix} 1 & 0 & 0 \\ 0 & \cos t & \sin t \\ 0 & -\sin t & \cos t \end{pmatrix}, & t \in [0, 2\pi], \\ \begin{pmatrix} \cos t & 0 & \sin t \\ 0 & 1 & 0 \\ -\sin t & 0 & \cos t \end{pmatrix}, & t \in (2\pi, 4\pi]. \end{cases}$$

The Banach indicatrix $\operatorname{Card}\left(T^{-1}(\mathbf{y})\right)$ equals 2 if $\mathbf{y}$ lies in the overlap of the two solid tori, and equals 1 otherwise. For reasons of symmetry, half a rotation of the object about each axis is actually enough to compute $f_{\mathcal{Y}}$ if f is real-valued, similar to Example 5.9.

6. Numerics

6.1. Discretization. For discretizing the filtered backpropagation formulae of Sections 5.1 and 5.2, we extend the approach of [28] to our general setting with some modifications for the Banach indicatrix. We consider the time steps $t_n := nL/N$ for $n = 1, \dots, N$, and quadrature points $\mathbf{x}_m \in \mathcal{B}_1^{d-1}$ for $m = 1, \dots, M$ that lie on a uniform grid. From (5.7), we obtain the *discrete backpropagation*

$$f_{\mathcal{Y}}(\mathbf{r}) \approx (2\pi)^{-\frac{1+d}{2}} \frac{|\mathcal{B}_{k_0}^{d-1}|\, L}{MN} \sum_{m=1}^{M} \sum_{n=1}^{N} \frac{2\kappa(\mathbf{z}_{m,n}) \mathrm{e}^{\mathrm{i}T(\mathbf{z}_{m,n})\cdot\mathbf{r}}\, \tilde{\mathcal{F}} u_t(k_0\mathbf{x}_m, r_{\mathrm{M}})\, |\det\left(\nabla T(\mathbf{z}_{m,n})\right)|}{k_0^2(t_n)\, \mathrm{i}\mathrm{e}^{\mathrm{i}\kappa(\mathbf{z}_{m,n})r_{\mathrm{M}}} \operatorname{Card}(T^{-1}(T(\mathbf{z}_{m,n})))}, \tag{6.1}$$

where $\mathbf{z}_{m,n} := (k_0(t_n)\mathbf{x}_m, t_n)$. For a non-absorbing object as of Theorem 5.5, we approximate $f_{\mathcal{Y}_{\mathrm{sym}}}$ analogously to (6.1), where we replace $\operatorname{Card}(T^{-1}(\cdot))$ by $\operatorname{Card}(T_{\mathrm{sym}}^{-1}(\cdot))$ and take twice the real part of the sum. We evaluate $f_{\mathcal{Y}}$ on a uniform grid

$$\mathbf{r}_{\mathbf{p}} = 2r_{\mathrm{M}}\mathbf{p}, \qquad \mathbf{p} \in \mathcal{I}_P^d := \{-\tfrac{P}{2}, \dots, \tfrac{P}{2} - 1\}^d, \tag{6.2}$$

for $P \in \mathbb{N}$. The *nonuniform discrete Fourier transform* (NDFT) $\mathbf{A}\colon \mathbb{C}^{P^d} \to \mathbb{C}^J$ of a vector $\mathbf{f} \in \mathbb{C}^{P^d}$ at points $\mathbf{y}_j \in \mathbb{R}^d$, $j = 1, \dots, J$, and its adjoint $\mathbf{A}^*\colon \mathbb{C}^J \to \mathbb{C}^{P^d}$ of $\mathbf{a} \in \mathbb{C}^j$ are defined by

$$(\mathbf{A}\mathbf{f})_j := \sum_{\mathbf{p}\in\mathcal{I}_P^d} \mathbf{f}_{\mathbf{p}}\, \mathrm{e}^{\mathrm{i}\mathbf{y}_j\cdot\mathbf{p}}, \qquad (\mathbf{A}^*\mathbf{a})_{\mathbf{p}} := \sum_{j=1}^{J} \mathbf{a}_j\, \mathrm{e}^{\mathrm{i}\mathbf{y}_j\cdot\mathbf{p}}.$$

With appropriate scaling and the enumeration $\mathbf{y}_{j(m,n)} = T(\mathbf{z}_{m,n})$, the evaluation of (6.1) corresponds to an adjoint NDFT, which can be computed efficiently in $\mathcal{O}(P^d \log P + NM)$ arithmetic operations, see [41, Chap. 7]. The Jacobian determinant $|\det(\nabla T)|$, see (5.8), can be approximated using finite differences.

Banach indicatrix The only part of (6.1) that is, in general, hard to determine analytically is the Banach indicatrix $\operatorname{Card}(T^{-1}(\mathbf{y}))$, which we approximate as follows. For simplicity, we only look at the case of continuous parameters, but we may apply the procedure for finitely many subintervals of t. The indicatrix counts how often a point $\mathbf{y} \in \mathcal{B}_{2k_0}^d$ is "hit" by the transformation T. In the discrete setting, however, it is unlikely that a point $\mathbf{y}$ is exactly hit by $T(\mathbf{z}_{m,n})$ for any m, n. By (5.3), we can express the coverage for fixed time t as the hemisphere

$$\left\{T(\mathbf{x}, t) : \mathbf{x} \in \mathcal{B}_{k_0}^{d-1}\right\} = \left\{\mathbf{y} \in \mathbb{R}^d : |\mathbf{y} + k_0(t)R(t)\mathbf{s}(t)| = k_0(t),\, \mathbf{y}\cdot R(t)\mathbf{e}^d > -k_0(t)\mathbf{s}(t)\cdot\mathbf{e}^d\right\}, \tag{6.3}$$

which moves continuously with t. For sufficiently close time steps, a point $\mathbf{y}$ is hit by T between the time steps t_{n-1} and t_n if the sign of $|\mathbf{y} + k_0(t)R(t)\mathbf{s}(t)| - k_0(t)$ changes between these time steps. Hence, we approximate $\operatorname{Card}(T^{-1}(\mathbf{y}))$ by

$$\sum_{n=1}^{N} \frac{s(n)}{2} \left|\operatorname{sgn}\left(|\mathbf{y} + k_0(t_{n-1})R(t_{n-1})\mathbf{s}(t_{n-1})| - k_0(t_{n-1})\right) - \operatorname{sgn}\left(|\mathbf{y} + k_0(t_n)R(t_n)\mathbf{s}(t_n)| - k_0(t_n)\right)\right|, \tag{6.4}$$

where the sign function is given in (5.13) and

$$s(n) := \begin{cases} 1, & \text{if } \mathbf{y} \cdot (R(t)\mathbf{e}^d) > -k_0(t_n)\mathbf{s}(t_n) \cdot \mathbf{e}^d, \\ 0, & \text{otherwise.} \end{cases}$$

Here the factor 1/2 compensates the fact that a full sign change of the argument changes the $\operatorname{sgn}(\cdot)$ function by 2.

Inverse NDFT and density compensation We compare the discrete backpropagation with other approaches. The forward model (4.3), which maps f to $\tilde{\mathcal{F}} u_t(\cdot, r_{\mathrm{M}})$, can be discretized via an NDFT: with the equispaced grid $\mathbf{r}_\mathbf{p}$ from (6.2), we have

$$\tilde{\mathcal{F}} u_{t_n}(\mathbf{x}_m, r_{\mathrm{M}}) \approx \left(\frac{2r_{\mathrm{M}}}{P}\right)^d \sqrt{\frac{\pi}{2}} \frac{\mathrm{i}\mathrm{e}^{\mathrm{i}\kappa r_{\mathrm{M}}}}{\kappa} k_0^2 \sum_{\mathbf{p} \in \mathcal{I}_P^d} \mathrm{e}^{-\mathrm{i}T(\mathbf{z}_{m,n}) \cdot \mathbf{r}_\mathbf{p}} f(\mathbf{r}_\mathbf{p}) \,. \tag{6.5}$$

The *inverse NDFT* method [28] consists in applying a conjugate gradient (CG) method to solve $\mathbf{A}\mathbf{f} = \mathbf{g}$, where

$$\mathbf{g} = \left(\tilde{\mathcal{F}} u_{t_n}(\mathbf{x}_m, r_{\mathrm{M}}) \left(\frac{P}{2r_{\mathrm{M}}}\right)^d \frac{-\mathrm{i}\sqrt{2}\,\kappa \mathrm{e}^{-\mathrm{i}\kappa r_{\mathrm{M}}}}{\sqrt{\pi}\, k_0^2} \right)_{m,n=1}^{M,N}$$

consists of the Fourier-transformed measurements, $\mathbf{f} = (f(\mathbf{r}_\mathbf{p}))_{\mathbf{p} \in \mathcal{I}_P^d}$, and $\mathbf{A}$ is the NDFT. Note that our implementation of the inverse NDFT enforces f to be real-valued as described in [2, sect. 5.2].

There are different approaches for numerical inversion of the NDFT, see [1, 16] and [25, sect. 3]. Furthermore, we consider the adjoint NDFT with *density compensation* factors that can be computed from $\mathbf{y}_{m,n}$ via a conjugate gradient (CG) method, see [26]. These factors play the same role as the weights in the backpropagation formula (6.1) because they only depend on the measurement setup, i.e. the transformation T, but not on the measured data u_t, and can therefore be precomputed.

6.2. Numerical tests. We consider a two-dimensional, real-valued test function $f \in L^1(\mathbb{R}^2)$ that contains both convex and nonconvex shapes, see Figure 9. Note that, different from [28], we plot the normalized scattering potential f, see (1.4). We discretize f on a 144×144 grid and take a fixed wave number $k_0 = 2\pi$ and the measurement line $x_2 = r_{\mathrm{M}} = 20$. Both for the inverse NDFT and the density compensation, we perform 20 CG iterations, the same as in [28]. We use the library [22, 23] for the (adjoint) NDFT in all tested algorithms. As our main goal is to examine the different backpropagation formulae, we generate the sinogram data $u_t(x, r_{\mathrm{M}})$ with the same forward model (6.5). In practice, one measures the total field $u_t^{\mathrm{tot}}(x, r_{\mathrm{M}}) := u_t(x, r_{\mathrm{M}}) + \mathrm{e}^{\mathrm{i}k_0 \mathbf{s}(t) \cdot (x, r_{\mathrm{M}})}$, i.e., the sum of the scattered field and incident field.

Angle scan We first consider an angle scanning setup, see Section 4.1, with a fixed position of the object, $R(t) = \mathrm{id}$, and the incidence direction $\mathbf{s}(t) = \mathbf{s}_0(t)/|\mathbf{s}_0(t)|$, where $\mathbf{s}_0(t) = (t - 1.2, 1)$ for $t \in [0, 2.4]$ with $N = 128$ time steps. We discretize x on the equispaced grid $2M^{-1}\mathcal{I}_M^1$ with $M = 128$. Figure 9b depicts the simulated sinogram $u_t^{\mathrm{tot}}(x)$. We always take the real part of the reconstructions of f and compare the quality using the peak signal-to-noise ratio (PSNR) and structural similarity index measure (SSIM).

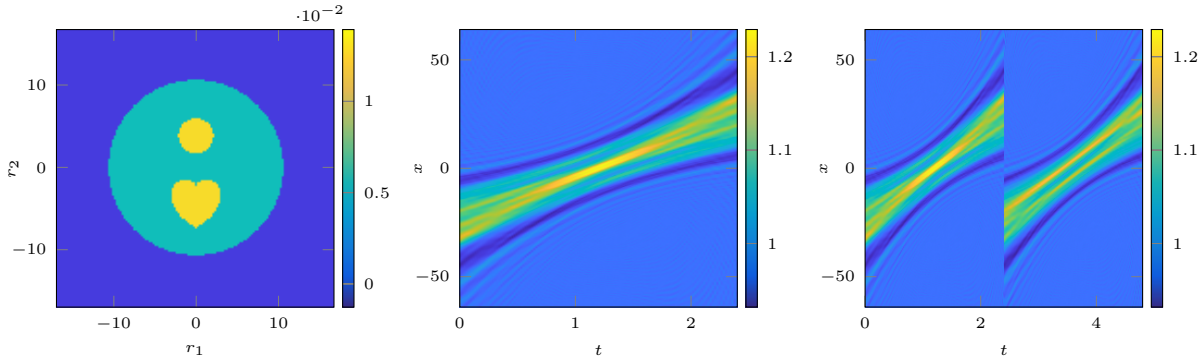

(a) *Function f* (b) *Sinogram for Figure 10 (angle scan)* (c) *Sinogram for Figure 11 (two angle scans combined)*

FIGURE 9. *Ground truth f (left) and absolute value of the sinograms $\left|u_t^{\mathrm{tot}}(x, r_{\mathrm{M}})\right|$.*

Figure 10 shows the reconstructions, the Fourier coverage $\mathcal{Y}$ and $\mathcal{Y}_{\mathrm{sym}}$, and the respective Banach indicatrix $\mathrm{Card}(T^{-1}(\mathbf{y}))$ or $\mathrm{Card}(T_{\mathrm{sym}}^{-1}(\mathbf{y}))$ estimated via (6.4). Both the backpropagation (6.1) and its symmetrized version yield similar results: they reveal the correct structure of the object, but underestimate the values of f. Moreover, they produce some artifacts due to the missing parts in the Fourier coverage, also known as the "missing cone", cf. [29]. The inverse NDFT gives a better reconstruction with the correct level of the peaks of f, but still shows some missing cone artifacts shaped similarly as in the backpropagation. The density compensation, which yields the largest error, overestimates the function and produces smoother artifacts that makes the two inclusions almost seem like a single large one.

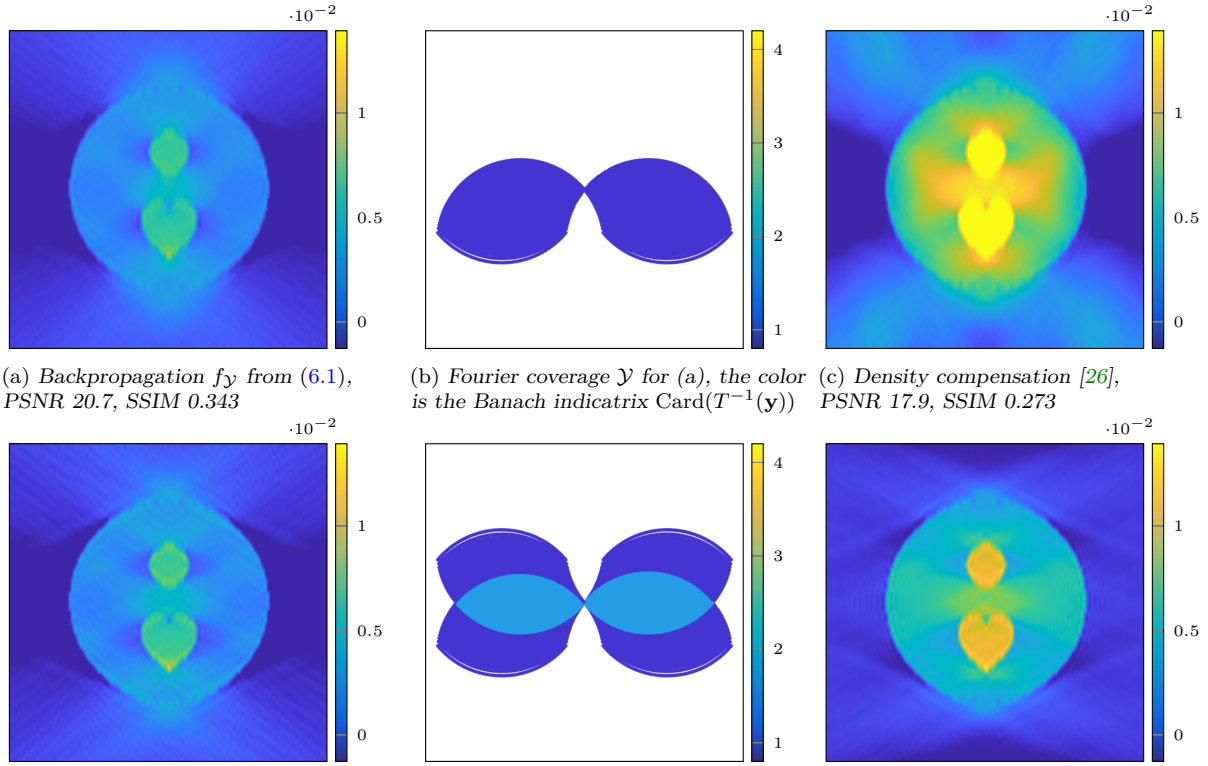

(a) *Backpropagation $f_{\mathcal{Y}}$ from (6.1), PSNR 20.7, SSIM 0.343*

(b) *Fourier coverage $\mathcal{Y}$ for (a), the color is the Banach indicatrix $\mathrm{Card}(T^{-1}(\mathbf{y}))$*

(c) *Density compensation [26], PSNR 17.9, SSIM 0.273*

(d) *Backpropagation $f_{\mathcal{Y}_{\mathrm{sym}}}$ with symmetrization, PSNR 20.9, SSIM 0.323*

(e) *Banach indicatrix $\mathrm{Card}(T_{\mathrm{sym}}^{-1}(\mathbf{y}))$ and Fourier coverage $\mathcal{Y}_{\mathrm{sym}}$ for (d)*

(f) *Inverse NDFT [28], PSNR 28.0, SSIM 0.593*

FIGURE 10. *Reconstructions for angle scan with fixed object. For comparison, we also show the inverse NDFT [28] and the density compensation [26].*

Angle scan and 90° rotation Our second setup demonstrates the necessity of non-smooth parameters. We take the above experiment, repeat it with the object rotated by 90°, and combine the data of both parts. Formally, we set $\mathbf{s}(t) = \mathbf{s}_0(t)/|\mathbf{s}_0(t)|$ where $\mathbf{s}_0(t) = (\alpha(t), 1)$ with

$$\begin{aligned} \alpha(t) &= t - 1.2 \quad \text{and} \quad R(t) = \left(\begin{smallmatrix} 1 & 0 \\ 0 & 1 \end{smallmatrix}\right) \quad \text{if } t \in [0, 2.4), \\ \alpha(t) &= t - 3.6 \quad \text{and} \quad R(t) = \left(\begin{smallmatrix} 0 & 1 \\ -1 & 0 \end{smallmatrix}\right) \quad \text{if } t \in [2.4, 4.8]. \end{aligned}$$

The sinogram $u_t^{\text{tot}}(x, r_{\text{M}})$ in Figure 9c shows the discontinuity at $t = 2.4$. The reconstructions are plotted in Figure 11. Again, the backpropagation yields better results than the density compensation. We see that the symmetrized backpropagation in Figure 11d gives a slightly better reconstruction than the one without in Figure 11a and is almost comparable with the inverse NDFT in Figure 11f. Furthermore, Figure 12 indicates that the backpropagation becomes considerably worse without the Banach indicatrix.

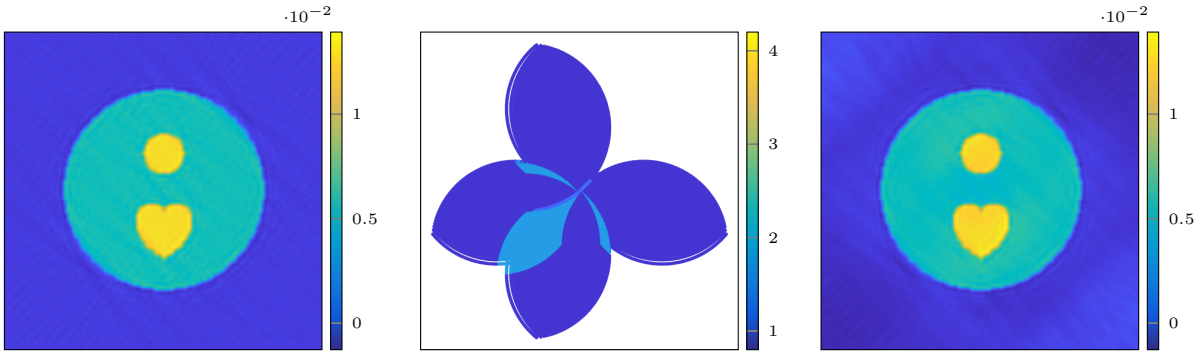

(a) *Backpropagation* $f_{\mathcal{Y}}$ *from* (6.1), *PSNR 37.5, SSIM 0.958*

(b) *Fourier coverage* $\mathcal{Y}$ *for (a), the color is the Banach indicatrix* $\text{Card}(T^{-1}(\mathbf{y}))$

(c) *Density compensation [26], PSNR 33.8, SSIM 0.624*

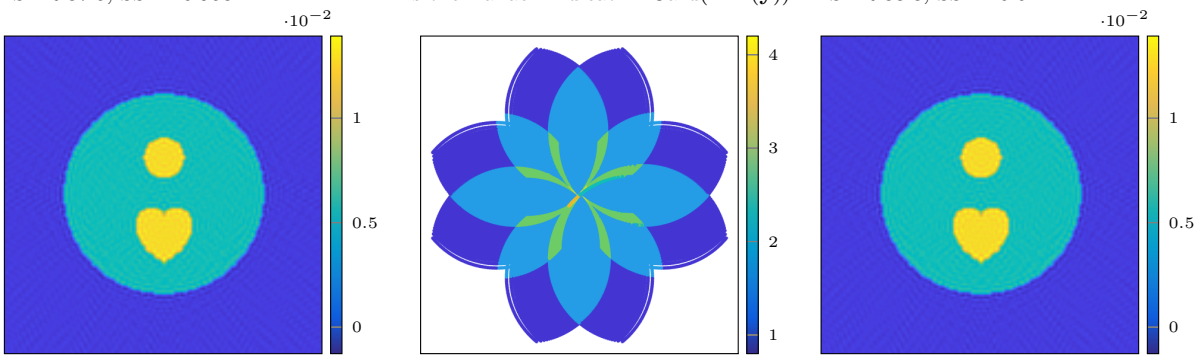

(d) *Symmetrized Backpropagation* $f_{\mathcal{Y}_{\text{sym}}}$ *from* (5.14), *PSNR 38.3, SSIM 0.958*

(e) *Banach indicatrix* $\text{Card}(T_{\text{sym}}^{-1}(\mathbf{y}))$ *and Fourier coverage* $\mathcal{Y}_{\text{sym}}$ *for (d)*

(f) *Inverse NDFT [28], PSNR 38.5, SSIM 0.980*

FIGURE 11. *Two angle scans combined: the first scan for the initial object, the second scan with the object rotated by 90°.*

To evaluate the stability of the algorithms, we repeat the above simulation and add Gaussian white noise to the measured sinogram of the total field u_t^{tot} with a relative noise level of 1 %, i.e., $\|u_{\text{noisy}}^{\text{tot}} - u^{\text{tot}}\| / \|u^{\text{tot}}\| \approx 1\,\%$ with the discrete L^2 norm $\|u^{\text{tot}}\| = (\sum_{n,m=1}^{N,M} |u_{t_n}^{\text{tot}}(x_m, r_{\text{M}})|^2)^{1/2}$. Note that the noise level relative to the scattered field $u = u^{\text{tot}} - u^{\text{inc}}$ is larger, namely $\|u_{\text{noisy}} - u\| / \|u\| \approx 5.8\,\%$. For the reconstructions in Figure 13 (a)–(d), we did not apply further regularization. All methods yield visually similar results: they correctly reconstruct the right shape and amplitude, but are distorted by some noise artifacts distributed almost equally over the image. Only the density compensation has structural artifacts visible in the background. The error metrics are best for the backpropagation $f_{\mathcal{Y}}$ by a small margin. As in [2], we post-process the noisy reconstructions via total variation (TV) denoising and enforcing the non-negativity of the reconstruction. In particular, we employ primal-dual splitting [6] to minimize

$$f \mapsto \tfrac{1}{2} \|f - f_{\mathcal{Y}}\|_{L^2}^2 + \lambda \|f\|_{\text{TV}} + \chi_{\geqslant 0}(f), \tag{6.6}$$

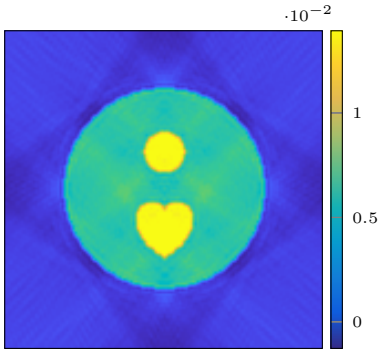

FIGURE 12. *Backpropagation $f_{\mathcal{Y}}$ for constant indicatrix, i.e., we use (5.7) with* $\mathrm{Card}(T_{\mathrm{sym}}^{-1}(\cdot)) \equiv 1$, *otherwise same setup as in Figure 11. PSNR 31.2, SSIM 0.605*

where $f_{\mathcal{Y}}$ is the backpropagation, $\lambda > 0$ a regularization parameter, $\|\cdot\|_{\mathrm{TV}}$ the total variation seminorm, and $\chi_{\geqslant 0}(f) = 0$ if $f \geqslant 0$ everywhere and $+\infty$ otherwise. The denoised images shown in Figure 13 (e)–(h) are significantly better. Again, all methods perform on a similar level. Noteworthy, the symmetrized backpropagation $f_{\mathcal{Y}_{\mathrm{sym}}}$ profits the most from denoising, even slightly beating the denoised inverse NDFT.

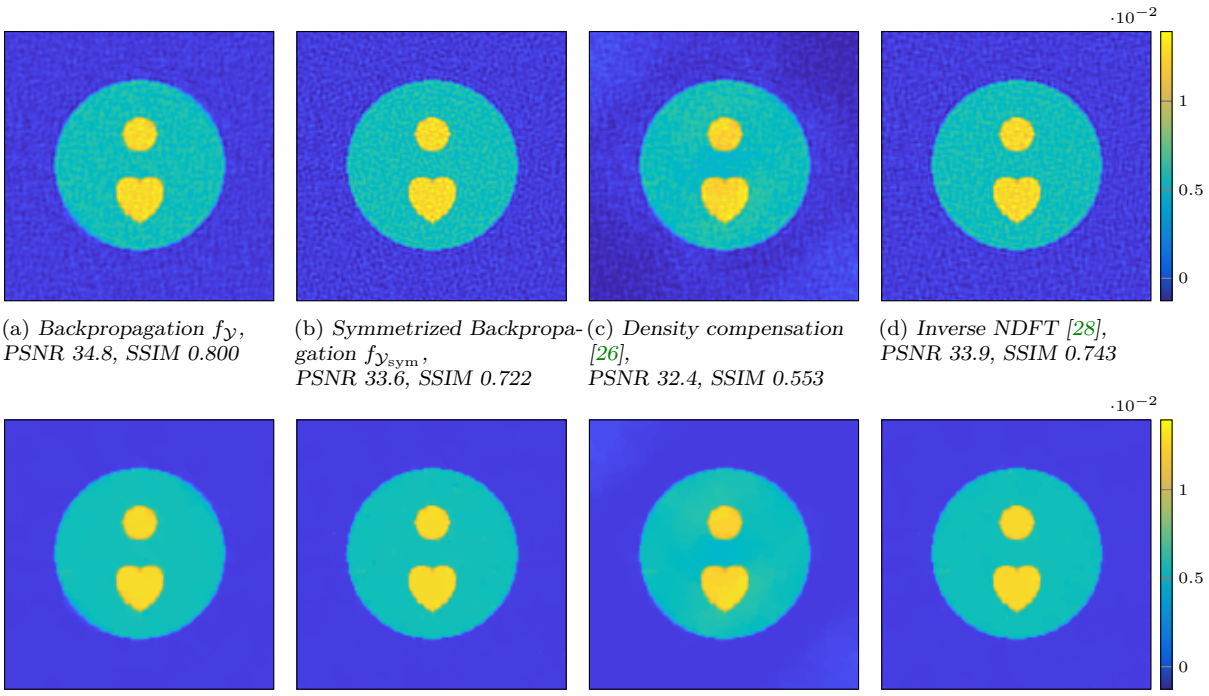

(a) *Backpropagation $f_{\mathcal{Y}}$, PSNR 34.8, SSIM 0.800*

(b) *Symmetrized Backpropagation $f_{\mathcal{Y}_{\mathrm{sym}}}$, PSNR 33.6, SSIM 0.722*

(c) *Density compensation [26], PSNR 32.4, SSIM 0.553*

(d) *Inverse NDFT [28], PSNR 33.9, SSIM 0.743*

(e) *TV denoising of backpropagation $f_{\mathcal{Y}}$, PSNR 37.8, SSIM 0.976*

(f) *TV denoising of symmetrized backpropagation $f_{\mathcal{Y}_{\mathrm{sym}}}$, PSNR 39.5, SSIM 0.982*

(g) *TV denoising of density compensation [26], PSNR 36.4, SSIM 0.900*

(h) *TV denoising of inverse NDFT [28], PSNR 38.9, SSIM 0.980*

FIGURE 13. *Reconstructions with 1 % Gaussian noise added to the sinogram u_t^{tot}. In the second row, we post-processed the reconstructions from the first row via TV denoising (6.6) with $\lambda = 0.02$. Otherwise, the setup is the same as in Figure 11.*

The computation times on an Intel Core i7-10700 CPU with 32 GB memory are reported in Table 1. As expected, the backpropagation algorithms are much faster, because they use only one adjoint NDFT whereas the inverse NDFT method uses a forward and adjoint step of the NDFT in each iteration. The precomputation of the Banach indicatrix and the Jacobian determinant, which is independent of the data u, is done in reasonable time. Note that here we do not include the time of the precomputation step inside the NFFT library, because it is required in all four

algorithms.

	Backpropagation	Symmetrized backpropagation	Density compensation	Inverse NDFT
Time	11	11	11	202
Precomputation	89	142	190	–

TABLE 1. *Computation times (in ms) for Figure 11.*

Object rotation In our third setup, we take the fixed incidence $\mathbf{s} = (0, 1)$ and the rotation $R(t) = \left(\begin{smallmatrix} \cos t & -\sin t \\ \sin t & \cos t \end{smallmatrix}\right)$ for $t \in [0, 3\pi/2]$ as in Figure 4c. Here the reconstruction highly depends on the discretization of x near the boundary. Therefore we use a different grid $x_m = \cos(\pi m/M)$ for $m = 1, \dots, M = 160$, such that the discrete Fourier coverage $\{T(x_m, t_n)\}_{m,n=1}^{M,N}$ does not have large gaps around the origin. The reconstructions are shown in Figure 14, where we can see a significant effect of the symmetrization. This is expected as the Fourier coverage $\mathcal{Y}$ has large gaps, see Figure 14b, but its symmetrization $\mathcal{Y}_{\text{sym}}$ from (5.11) is the whole disk of radius $2k_0$. The visual quality of the symmetrized backpropagation is comparably to the inverse NDFT, but the error measures are somewhat worse. Furthermore, we notice some numerical issues of the estimation of the Banach indicatrix $\text{Card}(T^{-1}(\mathbf{y}))$ near the boundary $|\mathbf{y}| = 2\pi$ corresponding to $|x| = 1$.

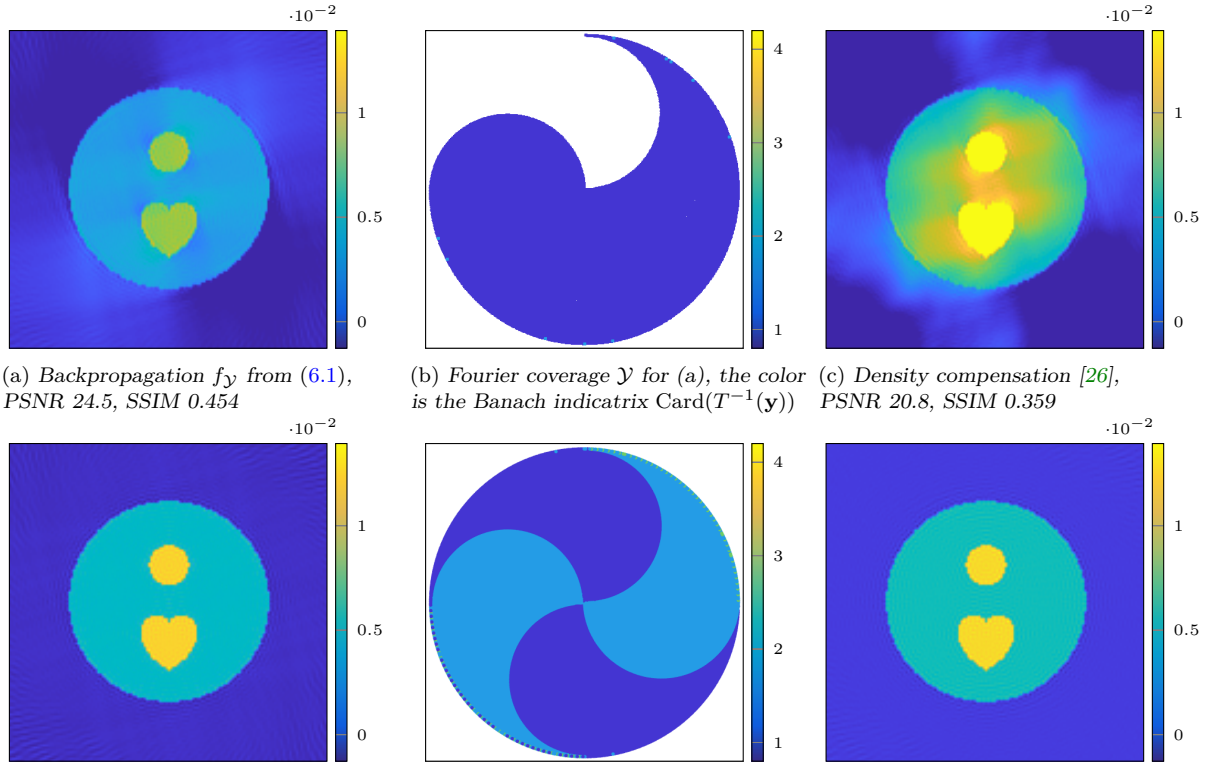

(a) *Backpropagation $f_{\mathcal{Y}}$ from (6.1), PSNR 24.5, SSIM 0.454*

(b) *Fourier coverage $\mathcal{Y}$ for (a), the color is the Banach indicatrix $\text{Card}(T^{-1}(\mathbf{y}))$*

(c) *Density compensation [26], PSNR 20.8, SSIM 0.359*

(d) *Backpropagation $f_{\mathcal{Y}_{\text{sym}}}$ with symmetrization, PSNR 32.5, SSIM 0.410*

(e) *Banach indicatrix $\text{Card}(T_{\text{sym}}^{-1}(\mathbf{y}))$ and Fourier coverage $\mathcal{Y}_{\text{sym}}$ for (d)*

(f) *Inverse NDFT [28], PSNR 41.9, SSIM 0.983*

FIGURE 14. *Reconstructions for setup of Figure 4c. For comparison, we also show the inverse NDFT [28] and the density compensation [26].*

7. Conclusion

In this article we have studied several questions related to diffraction tomography in $\mathbb{R}^d$. We derived a generalization of the Fourier diffraction theorem for compactly supported inhomogeneity $g \in L^1(\mathbb{R}^d)$ and a measurement hyperplane that may intersect $\operatorname{supp} g$. Building on this result, we presented a novel filtered backpropagation formula, that is, an explicit expression for the L^2 best approximation of f given the available data. This reconstruction formula correctly handles a general experiment where a change of illumination and a rigid motion of the object occur simultaneously. The critical quantity in the evaluation of the resulting d-dimensional integral is the Banach indicatrix, which can be difficult to determine exactly. We have addressed this issue with a numerical estimation method. Numerical tests suggest that the filtered backpropagation formula can compete with the inverse NDFT in terms of reconstruction quality, while having lower computation times.

Acknowledgments. This work is supported by the Austrian Science Fund (FWF), SFB 10.55776/F68 ("Tomography across the Scales"), and by the German Research Foundation DFG (STE 571/19-1, project number 495365311). The financial support by the Austrian Federal Ministry for Digital and Economic Affairs, the National Foundation for Research, Technology and Development and the Christian Doppler Research Association is gratefully acknowledged. This work was initiated while the third-named author was with the Johann Radon Institute for Computational and Applied Mathematics (RICAM) of the Austrian Academy of Sciences.

References

[1] B. Adcock, M. Gataric, and A. Hansen. "On Stable Reconstructions from Nonuniform Fourier Measurements". In: *SIAM Journal on Imaging Sciences* 7.3 (2014), pp. 1690–1723. DOI: 10.1137/130943431 (cited on page 25).

[2] R. Beinert and M. Quellmalz. "Total Variation-Based Reconstruction and Phase Retrieval for Diffraction Tomography". In: *SIAM Journal on Imaging Sciences* 15.3 (2022), pp. 1373–1399. DOI: 10.1137/22m1474382 (cited on pages 4, 19, 25, 27).

[3] R. Beinert and M. Quellmalz. "Total Variation-Based Reconstruction and Phase Retrieval for Diffraction Tomography with an Arbitrarily Moving Object". In: *Proceedings in Applied Mathematics and Mechanics* 22.1 (2023). DOI: 10.1002/pamm.202200135 (cited on page 4).

[4] V. Bogachev. "Measure Theory". Vol. 1. Springer Berlin Heidelberg, 2007 (cited on page 17).

[5] M. Born and E. Wolf. "Principles of Optics". Seventh Anniversary Edition. Cambridge University Press, 2019. DOI: 10.1017/9781108769914 (cited on page 2).

[6] A. Chambolle, V. Caselles, D. Cremers, M. Novaga, and T. Pock. "An Introduction to Total Variation for Image Analysis". In: *Theoretical Foundations and Numerical Methods for Sparse Recovery*. Ed. by M. Fornasier. De Gruyter, 2010, pp. 263–340. DOI: 10.1515/9783110226157.263 (cited on page 27).

[7] D. Colton and R. Kress. "Inverse Acoustic and Electromagnetic Scattering Theory". 4th ed. Applied Mathematical Sciences 93. Springer, 2019. ISBN: 978-3-030-30350-1 (cited on pages 2, 5).

[8] R. Courant and D. Hilbert. "Methods of Mathematical Physics". Vol. 2. New York: Wiley-Interscience, 1962 (cited on pages 4, 5).

[9] A. Devaney. "A filtered backpropagation algorithm for diffraction tomography". In: *Ultrasonic Imaging* 4.4 (1982), pp. 336–350. DOI: 10.1016/0161-7346(82)90017-7 (cited on pages 2, 3, 16, 22, 23).

[10] A. J. Devaney. "Mathematical Foundations of Imaging, Tomography and Wavefield Inversion". Cambridge University Press, 2012. DOI: 10.1017/cbo9781139047838 (cited on page 3).

[11] G. Evequoz and T. Weth. "Dual variational methods and nonvanishing for the nonlinear Helmholtz equation". In: *Advances in Mathematics* 280 (2015), pp. 690–728. DOI: 10.1016/j.aim.2015.04.017 (cited on pages 6, 8).

[12] G. Evéquoz. "Existence and asymptotic behavior of standing waves of the nonlinear Helmholtz equation in the plane". In: *Analysis* 37.2 (2017), pp. 55–68. DOI: 10.1515/anly-2016-0023 (cited on page 6).

[13] F. Faucher, C. Kirisits, M. Quellmalz, O. Scherzer, and E. Setterqvist. "Diffraction Tomography, Fourier Reconstruction, and Full Waveform Inversion". In: *Handbook of Mathematical Models and Algorithms in Computer Vision and Imaging*. Ed. by K. Chen, C.-B. Schönlieb, X.-C. Tai, and L. Younces. Cham: Springer, 2023, pp. 273–312. DOI: 978-3-030-98661-2_115 (cited on page 2).

[14] H. Federer. "Geometric Measure Theory". Classics in Mathematics. Berlin: Springer Verlag, 1996 (cited on page 21).

[15] G. Folland. "Introduction to Partial Differential Equations". Princeton University Press, 1995 (cited on page 4).

[16] A. Gelb and G. Song. "A Frame Theoretic Approach to the Nonuniform Fast Fourier Transform". In: *SIAM Journal on Numerical Analysis* 52.3 (2014), pp. 1222–1242. DOI: 10.1137/13092160x (cited on page 25).

[17] I. S. Gradshteyn and I. M. Ryzhik. "Table of Integrals, Series, and Products". 7th ed. Academic Press New York, 2007 (cited on page 8).

[18] S. Gutiérrez. "Non trivial L^q solutions to the Ginzburg-Landau equation". In: *Mathematische Annalen* 328.1–2 (2004), pp. 1–25. DOI: 10.1007/s00208-003-0444-7 (cited on page 6).

[19] P. Hajłasz. "Change of variables formula under minimal assumptions". In: *Colloquium Mathematicae* 64.1 (1993), pp. 93–101. DOI: 10.4064/cm-64-1-93-101 (cited on page 17).

[20] L. Hörmander. "The Analysis of Linear Partial Differential Operators: Distribution Theory and Fourier Analysis". Springer, 1990. DOI: 10.1007/978-3-642-61497-2 (cited on page 10).

[21] A. C. Kak and M. Slaney. "Principles of Computerized Tomographic Imaging". Vol. 33. Classics in Applied Mathematics. Philadelphia, PA: Society for Industrial and Applied Mathematics (SIAM), 2001. DOI: 10.1137/1.9780898719277 (cited on pages 1–3, 11, 16, 22).

[22] J. Keiner, S. Kunis, and D. Potts. *NFFT 3.5, C subroutine library*. https://www.tu-chemnitz.de/~potts/nfft (cited on page 25).

[23] J. Keiner, S. Kunis, and D. Potts. "Using NFFT3 - a Software Library for Various Nonequispaced Fast Fourier Transforms". In: *ACM Trans. Math. Software* 36 (2009), Article 19, 1–30. DOI: 10.1145/1555386.1555388 (cited on page 25).

[24] C. E. Kenig, A. Ruiz, and C. D. Sogge. "Uniform Sobolev inequalities and unique continuation for second order constant coefficient differential operators". In: *Duke Mathematical Journal* 55.2 (1987). DOI: 10.1215/s0012-7094-87-05518-9 (cited on page 6).

[25] M. Kircheis and D. Potts. "Fast and direct inversion methods for the multivariate nonequispaced fast Fourier transform". In: *Frontiers in Applied Mathematics and Statistics* 9 (2023). DOI: 10.3389/fams.2023.1155484 (cited on page 25).

[26] M. Kircheis and D. Potts. "Optimal density compensation factors for the reconstruction of the Fourier transform of bandlimited functions". In: *Fourteenth International Conference on Sampling Theory and Applications*. 2023 (cited on pages 25–29).

[27] C. Kirisits, N. Naujoks, O. Scherzer, and H. Yang. "Diffraction tomography for incident Herglotz waves". In: *Inverse Problems* 40.11 (2024), p. 115007. DOI: 10.1088/1361-6420/ad7d2d (cited on page 12).

[28] C. Kirisits, M. Quellmalz, M. Ritsch-Marte, O. Scherzer, E. Setterqvist, and G. Steidl. "Fourier reconstruction for diffraction tomography of an object rotated into arbitrary orientations". In: *Inverse Problems* 37.11 (2021), p. 115002. DOI: 10.1088/1361-6420/ac2749 (cited on pages 2, 9, 16, 23–29).

[29] W. Krauze. "Optical diffraction tomography with finite object support for the minimization of missing cone artifacts". In: *Biomedical Optics Express* 11.4 (2020), pp. 1919–1926. DOI: 10.1364/BOE.386507 (cited on pages 3, 26).

[30] V. Lauer. "New approach to optical diffraction tomography yielding a vector equation of diffraction tomography and a novel tomographic microscope". In: *Journal of Microscopy* 205.2 (2002), pp. 165–176. DOI: 10.1046/j.0022-2720.2001.00980.x (cited on page 12).

[31] K. Lee, S. Shin, Z. Yaqoob, P. T. C. So, and Y. Park. "Low-coherent optical diffraction tomography by angle-scanning illumination". In: *Journal of Biophotonics* 12.5 (2019). DOI: 10.1002/jbio.201800289 (cited on page 13).

[32] M. Lee, K. Kim, J. Oh, and Y. Park. "Isotropically resolved label-free tomographic imaging based on tomographic moulds for optical trapping". In: *Light: Science & Applications* 10.1 (2021), p. 102. DOI: 10.1038/s41377-021-00535-4 (cited on page 3).

[33] J. Lim, K. Lee, K. H. Jin, S. Shin, S. Lee, Y. Park, and J. C. Ye. "Comparative study of iterative reconstruction algorithms for missing cone problems in optical diffraction tomography". In: *Optics Express* 23.13 (2015), p. 16933. DOI: 10.1364/oe.23.016933 (cited on page 3).

[34] J. Malý, D. Swanson, and W. P. Ziemer. "The co-area formula for Sobolev mappings". In: *Transactions of the American Mathematical Society* 35.2 (2002), pp. 77–492. DOI: 10.1364/JOSAA.35.001891 (cited on page 21).

[35] W. McLean. "Strong Elliptic Systems and Boundary Integral Equations". London: Cambridge University Press, 2000 (cited on pages 5, 8).

[36] B. Mejri and O. Scherzer. "An Inversion Scheme for Elastic Diffraction Tomography Based on Mode Separation". In: *SIAM Journal on Applied Mathematics* 84.1 (Feb. 2024), pp. 165–188. DOI: 10.1137/22M1538909 (cited on page 12).

[37] P. Müller, M. Schürmann, and J. Guck. *The Theory of Diffraction Tomography*. 2016. arXiv: 1507.00466 [q-bio.QM] (cited on pages 2, 19).

[38] F. Natterer and F. Wübbeling. "Mathematical Methods in Image Reconstruction". Monographs on Mathematical Modeling and Computation 5. Philadelphia, PA: SIAM, 2001 (cited on pages 1–3, 11).

[39] *NIST Digital Library of Mathematical Functions*. https://dlmf.nist.gov/, Release 1.1.11 of 2023-09-15 (cited on page 5).

[40] C. Park, S. Shin, and Y. Park. "Generalized quantification of three-dimensional resolution in optical diffraction tomography using the projection of maximal spatial bandwidths". In: *Journal of the Optical Society of America A* 35.11 (2018), pp. 1891–1898. DOI: 10.1364/JOSAA.35.001891 (cited on page 13).

[41] G. Plonka, D. Potts, G. Steidl, and M. Tasche. "Numerical Fourier Analysis". Applied and Numerical Harmonic Analysis. Birkhäuser, 2018. DOI: 10.1007/978-3-030-04306-3 (cited on page 24).

[42] M. Quellmalz, P. Elbau, O. Scherzer, and G. Steidl. "Motion detection in diffraction tomography by common circle methods". In: *Mathematics of Compation* 93.346 (2024), pp. 747–784. DOI: 10.1090/mcom/3869 (cited on page 13).

[43] F. Rellich. "Über das asymptotische Verhalten der Lösungen von $\Delta u + \lambda u = 0$ in unendlichen Gebieten." In: *Jahresbericht der Deutschen Mathematiker-Vereinigung* 53 (1943), pp. 57–65 (cited on page 5).

[44] W. Rudin. "Real and Complex Analysis". 3rd ed. New York: McGraw-Hill, 1987 (cited on page 18).

[45] M. G. Slaney. "Imaging with Diffraction Tomography". PhD thesis. Purdue University, 1985 (cited on page 22).

[46] A. Sommerfeld. "Die Greensche Funktion der Schwingungslgleichung". In: *Jahresbericht der Deutschen Mathematiker-Vereinigung* 21 (1912), pp. 309–352 (cited on page 5).

[47] Y. Sung and R. R. Dasari. "Deterministic regularization of three-dimensional optical diffraction tomography". In: *Journal of the Optical Society of America A* 28.8 (2011), p. 1554. DOI: 10.1364/josaa.28.001554 (cited on page 3).

[48] E. Wolf. "Three-dimensional structure determination of semi-transparent objects from holographic data". In: *Optics Communications* 1 (1969), pp. 153–156 (cited on pages 1, 2, 11, 16).